the sensitivity of recent conclusions[16] about mode selectivity in S_N2 reactions to variations in the potential energy function.

Acknowledgment. We are grateful to Maurice Kreevoy for helpful discussions. This work was supported in part by the U.S. Department of Energy, Office of Basic Energy Sciences and the Minnesota Supercomputer Institute.

Registry No. Cl, 16887-00-6; CH_3Cl, 74-87-3; D, 7782-39-0; Cl_2, 7782-50-5.

Supplementary Material Available: A description of the method used to determine the coefficients for g_{ij}, eq 31, and a listing of the force constant matrix (16 pages). Ordering information is given on any current masthead page.

Effect of Nonequilibrium Solvation on Chemical Reaction Rates. Variational Transition-State-Theory Studies of the Microsolvated Reaction $Cl^-(H_2O)_n + CH_3Cl$

Susan C. Tucker and Donald G. Truhlar*

Contribution from the Department of Chemistry and Supercomputer Institute, University of Minnesota, Minneapolis, Minnesota 55455-0431. *Received July 24, 1989*

Abstract: We present a potential energy surface for the microhydrated S_N2 reaction of a chloride ion with methyl chloride in the presence of one or two water molecules. All degrees of freedom are included. We analyze the stationary points corresponding to reactant, ion–dipole complex, and transition state for the monohydrated and the dihydrated reactions, and we use generalized transition-state theory to evaluate the rate constants for these reactions. A noteworthy feature of the dynamics calculations is that vibrational zero point effects are included, as are effects of quantization on vibrational heat capacities and entropies, and water molecules are treated as nonrigid. We find that the rate constant at 300 K decreases from the gas-phase value of 3.5×10^{-14} cm^3 molecule^{-1} s^{-1} to a value of 1.1×10^{-17} cm^3 molecule^{-1} s^{-1} for the monohydrated reaction and to a value of 3.7×10^{-20} cm^3 molecule^{-1} s^{-1} for the dihydrated reaction. We have also evaluated the rate constant for the monohydrated reaction under the equilibrium solvation approximation. The extent of nonequilibrium solvation is tested by comparing calculations in which the water molecule degrees of freedom participate in the reaction coordinate to those in which they do not. Two different methods for defining the generalized transition-state theory dividing surface under the equilibrium solvation approximation lead to quite different values for the equilibrium solvation rate constant, and we determine which equilibrium solvation approximation is more appropriate by using variational transition-state theory.

1. Introduction

The study of solvent effects on chemical reaction rates has a long history, and it has played a central role in recent work examining the applicability of transition-state theory to reactions in solution, as discussed in recent reviews.[1-3] Theoretical interpretation of bimolecular nucleophilic substitution (S_N2) reactions also has a long history,[4,5] and these reactions have become the prototype for recent work on solvent effects. In particular, the reaction of chloride with methyl chloride has received considerable recent attention.[6-22] Two strong themes distinguishing the modern work from the classical studies[23] are (i) the comparison of ionic reaction kinetics in solution to data on the same reactions as they occur with uncomplexed reagents in the gas phase[8-15,21,22] and (ii) quantitative studies of microsolvated species, i.e., clusters, as a bridge between the gas phase and solution.[6,11,24-29] This paper is a detailed study of the effect of microsolvation, in particular microhydration, on the prototype S_N2 reaction of chloride and methyl chloride, using variational transition-state theory (VTST)[1,3,13,16,17,30-35] and a potential energy surface in which all

(1) Truhlar, D. G.; Hase, W. L.; Hynes, J. T. *J. Phys. Chem.* **1983**, *87*, 2664, 5523(E).
(2) Hynes, J. T. In *Theory of Chemical Reaction Dynamics*; Baer, M., Ed.; CRC Press: Boca Raton, FL, 1985; Vol. 4, p 171.
(3) Kreevoy, M. M.; Truhlar, D. G. In *Investigation of Rates and Mechanisms of Reactions* (*Techniques of Chemistry*, 4th ed.; Weissberger, A., Ed.; Vol. 6) Bernasconi, C. F., Ed.; John Wiley & Sons: New York, 1986; Part I, p 13.
(4) Dostrovsky, I.; Hughes, E. D.; Ingold, C. K. *J. Chem. Soc.* **1946**, 173.
(5) de la Mare, P. B. D.; Fowden, L.; Hughes, E. D.; Ingold, C. K., Mackie, J. D. H. *J. Chem. Soc.* **1955**, 3200.
(6) Morokuma, K. *J. Am. Chem. Soc.* **1982**, *104*, 3732.
(7) Bazilevskii, M. V.; Koldobskii, S. G. *Zh. Org. Khim.* **1984**, *20*, 908.
(8) Chandrasekhar, J.; Smith, S. F.; Jorgensen, W. L. *J. Am. Chem. Soc.* **1985**, *107*, 154.
(9) Shaik, S. S. *Prog. Phys. Org. Chem.* **1985**, *15*, 197.
(10) German, E. D.; Kuznetsov, A. M. *Faraday Trans. II* **1986**, *82*, 1885.
(11) Kong, Y. S.; Jhon, M. S. *Theor. Chim. Acta* **1986**, *70*, 123.
(12) Bergsma, J. P.; Gertner, B. J.; Wilson, K. R.; Hynes, J. T. *J. Chem. Phys.* **1987**, *86*, 1356.
(13) Gertner, B. J.; Bergsma, J. P.; Wilson, K. R.; Lee, S.; Hynes, J. T. *J. Chem. Phys.* **1987**, *86*, 1377.
(14) Bash, P. A.; Field, M. J.; Karplus, M. *J. Am. Chem. Soc.* **1987**, *109*, 8092.
(15) Burshtein, K. Y. *J. Mol. Struct.* **1987**, *153*, 209.
(16) Lee, S.; Hynes, J. T. *J. Chem. Phys.* **1983**, *88*, 6863.
(17) Hwang, J.-K.; King, G.; Creighton, S.; Warshel, A. *J. Am. Chem. Soc.* **1988**, *110*, 5297.
(18) Hwang, J.-K.; Creighton, S.; King, G.; Whitney, D.; Warshel, A. *J. Chem. Phys.* **1988**, *89*, 859.
(19) Gertner, B. J.; Wilson, K. R.; Hynes, J. T. *J. Chem. Phys.* **1989**, *90*, 3537.
(20) Kozaki, T.; Morishashi, K.; Kikuchi, O. *J. Am. Chem. Soc.* **1989**, *111*, 1547.
(21) Chiles, R. A.; Rossky, P. J. *J. Am. Chem. Soc.* **1984**, *106*, 6867. Huston, S. E.; Rossky, P. J.; Zichi, D. A. *J. Am. Chem. Soc.* In press.
(22) Tucker, S. C.; Truhlar, D. G. *Chem. Phys. Lett.* **1989**, *157*, 164.
(23) Hine, J. *Physical Organic Chemistry*; McGraw-Hill: New York, 1962.
(24) Bertrán, J. In *New Theoretical Concepts for Understanding Organic Reactions, NATO ASI Ser. C*; Bertrán, J., Csizmadia, I. G., Eds.; Kluwer Academic Publishers: Dordrecht, 1989, Vol. 267, p 231.
(25) Bohme, D. K.; Raskit, A. B. *J. Am. Chem. Soc.* **1984**, *106*, 3447.
(26) Bohme, D. K.; Raskit, A. B. *Can. J. Chem.* **1985**, *63*, 3007.
(27) Henchman, M.; Paulson, J. F.; Hierl, P. M. *J. Am. Chem. Soc.* **1983**, *105*, 5509.
(28) Henchman, M.; Hierl, P. M.; Paulson, J. F. *J. Am. Chem. Soc.* **1985**, *107*, 2812.
(29) Henchman, M.; Hierl, P. M.; Paulson, J. F. *ACS Adv. Chem. Ser.* **1987**, *215*, 83.

0002-7863/90/1512-3347$02.50/0 © 1990 American Chemical Society

degrees of freedom of both the reagents and the solvating molecules are included explicitly.

The effect of solvent molecules on chemical reactions can be classified into two different types of contributions. The first type, called static solvation effects, are contributions which do not require inclusion of the solvent coordinates in the reaction coordinate (the precise meaning of this statement is clarified in section 4); static solvation effects can be incorporated into reaction rate calculations by letting the solvent equilibrate for each given geometry of the solute or—more approximately—by an equilibrium continuum model. When solvation effects are included in transition-state theory calculations, static solvent effects are associated with solvent contributions to the free energy of activation along the equilibrium solvation path; this path is defined in coordinate space by assuming that, at each point on the solute reaction path determined in the absence of solvent, the solvent is equilibrated with the solute. These static solvent effects are therefore also called equilibrium solvation effects.

However, this kind of treatment will sometimes neglect important solvent–solute couplings. Solvent effects which require a more dynamical treatment of the solvent coordinates are called dynamic or nonequilibrium solvation effects. The phenomenon of nonequilibrium solvation has been discussed recently by Kurz, Hynes, and Warshel and their respective co-workers.[12,13,16,18,19,34,36-40] These discussions have suggested that the extent of equilibration of the solvent will be governed by the strength of the solute–solvent coupling, as given by the interaction force field, by the sharpness of the barrier, and by the characteristic time scales of solvent motion and solute reactive motion. In general, if the characteristic time scale for solvent reorganization is much slower than the time scale for solute reactive motion, nonequilibrium solvation effects on the rate constants are expected to be significant; however, the solvent–solute coupling strength is also paramount in determining the magnitude of these effects. One approach would suggest that strong solute–solvent interactions yield large nonequilibrium solvation effects because strong coupling allows the solvent to hinder reactive solute motion, but Kurz and Kurz[36] argue that strong solute–solvent coupling may lead to negligible nonequilibrium solvation effects because strong coupling forces the solvent to remain equilibrated with the solute, a concerted mechanism. In the case of weak coupling, Kurz and Kurz[36] suggest that time scale differences will cause a sequential mechanism. Motion along the equilibrium solvation path and nonequilibrium solvation effects may both involve concerted solvent and solute motions, and thus either may correspond to the "coupled mechanism" discussed by Kurz and co-workers.[36,37] The dynamics of the solute–solvent coupling has been explored in the framework of linear response theory by Hwang et al.,[18] who evaluated the solute–solvent coupling by including the solvent in the solute Hamiltonian in a simulation. Their interpretation of the results supports the view of Kurz and Kurz.[36]

Because these ideas of equilibrium and nonequilibrium solvation effects are central to solution-phase kinetics, it is worthwhile to attempt a more precise formulation, and this is one of the goals of the present work. In particular, we adapt a reaction-path formalism previously developed[30-32] for gas-phase variational transition-state theory for this purpose. We then evaluate the importance of nonequilibrium solvation effects on the microhydrated chloride plus methyl chloride system by comparing variational transition-state theory rate constants evaluated without assuming equilibrium solvation to those evaluated with equilibrium solvation enforced. We note that in the nonequilibrium solvation calculations presented here, deviations from the equilibrium solvation path are allowed to occur in the solute coordinates as well as in the solvent coordinates.

We begin, in section 2, by describing the analytic functions we use to represent the potential energy function and the charge switching of the microhydrated system. In section 3, we describe the calculated stationary points along the reaction paths of the monohydrated and the dihydrated systems. In section 4, we discuss how generalized transition-state theory is applied in a calculation in which all degrees of freedom of the interacting particles are considered explicitly, i.e., in a nonequilibrium solvation calculation. We then discuss two different methods for applying generalized transition-state theory when making the equilibrium solvation assumption.

We apply these methods to the microhydrated chloride plus methyl chloride reaction, and we give the details of the calculations in section 5. In section 6 we present results; section 6.1 gives reaction rate constants from nonequilibrium solvation calculations (i.e., VTST allowing all degrees of freedom to participate in the local reaction coordinate) for both the mono- and dihydrated reactions; section 6.2 gives the reaction rate constants for the monohydrated reaction reevaluated under the equilibrium solvation approximation by the two methods discussed in section 4, and we compare the results to the nonequilibrium solvation results for this reaction. We find that the two different methods for applying generalized transition-state theory with equilibrium solvation yield quite different results, we discuss why this is so, and we use the variational criterion of generalized transition-state theory to determine which is the better model. Finally, in section 7, we discuss the relevance of these results to other studies on the solvated chloride plus methyl chloride reaction and on nonequilibrium solvation effects in general.

2. Potential Energy Surfaces

We start with our semiempirical, multidimensional surface S for the gas-phase reaction

$$Cl^- + CH_3Cl' \rightarrow ClCH_3 + Cl'^- \qquad (R1)$$

which we described in the preceding paper.[41] We will use surface S as a building block for creating surfaces for the series of reactions

$$(H_2O)_n{\cdot}Cl^- + CH_3Cl' \rightarrow ClCH_3 + Cl'^-{\cdot}(H_2O)_n \qquad (R2)$$

In order to develop a full potential energy surface for reaction R2 with $n = 1$, we add an intramolecular water potential and a solute–solvent interaction potential, as discussed below. For $n > 1$, we also add an intermolecular water–water potential.

For the intermolecular water–water potential we use the RWK2 potential, V^{RWK2}, of Reimers et al.,[42] because it was designed to give interactions between deformable monomer units, and it has been shown to give reasonable values for experimental observables, when combined with a suitable intramolecular potential,[43] both for clusters of small numbers of water molecules[44] and for water in the bulk phase.[45] The ability of the model to represent both cluster and bulk phase water is quite desirable if one hopes eventually to gain an understanding of reactions in bulk solution by using large vales for n, the number of water molecules, in reaction R2.

For the intramolecular water potential, V^W, we use the coupled local mode potential of Coker, Miller, and Watts,[46] and we

(30) Garrett, B. C.; Truhlar, D. G. *J. Chem. Phys.* **1979**, *70*, 1593.
(31) Truhlar, D. G.; Garrett, B. C. *Acc. Chem. Res.* **1980**, *13*, 440.
(32) Truhlar, D. G.; Isaacson, A. D.; Garrett, B. C. In *The Theory of Chemical Reaction Dynamics*; Baer, M., Ed.; CRC Press: Boca Raton, FL, 1985; p 65.
(33) Ladanyi, B. M.; Hynes, J. T. *J. Am. Chem. Soc.* **1986**, *108*, 585.
(34) Lee, S.; Hynes, J. T. *J. Chem. Phys.* **1988**, *88*, 6853.
(35) Tucker, S. C.; Truhlar, D. G. In *New Theoretical Concepts for Understanding Organic Reactions, NATO ASI Ser. C*; Bertrán, J., Csizmadia, I. G., Eds.; Kluwer Academic Publishers: Dordrecht, 1989; Vol. 267, p 291.
(36) Kurz, J. L.; Kurz, L. C. *J. Am. Chem. Soc.* **1972**, *94*, 4451. Kurz, J. L.; Kurz, L. C. *Israel J. Chem.* **1985**, *26*, 339.
(37) Kurz, J. L.; Lee, J.; Love, M. E.; Rhodes, S. E. *J. Am. Chem. Soc.* **1986**, *108*, 2960.
(38) van der Zwan, G.; Hynes, J. T. *J. Chem. Phys.* **1982**, *76*, 2993.
(39) van der Zwan, G.; Hynes, J. T. *J. Chem. Phys.* **1983**, *78*, 4174.
(40) van der Zwan, G.; Hynes, J. T. *Chem. Phys.* **1984**, *90*, 21.
(41) Tucker, S. C.; Truhlar, D. G. Preceding paper in this issue.
(42) Reimers, J. R.; Watts, R. O.; Klein, M. L. *Chem. Phys.* **1982**, *64*, 95.
(43) Reimers, J. R.; Watts, R. O. *Mol. Phys.* **1984**, *52*, 357.
(44) Reimers, J. R.; Watts, R. O. *Chem. Phys.* **1984**, *85*, 83.
(45) Reimers, J. R.; Watts, R. O. *Chem. Phys.* **1984**, *91*, 201.
(46) Coker, D. F.; Miller, R. E.; Watts, R. O. *J. Chem. Phys.* **1985**, *82*, 3554.

combine it with the RWK2 intermolecular potential in the manner of Coker and Watts.[47] Because there are typographical errors in some of the original papers on these potentials,[42-45] we note that we take the potential form and parameters to be exactly as given in ref 47.

The RWK2 intermolecular potential is based on a sum of site–site interactions. It involves one site on each of the three atoms of H_2O for the short-range interactions and one site on each hydrogen plus a site displaced from the oxygen for the coulombic interactions; in the standard terminology, then, it is a "four-site" model. The combined inter- and intramolecular potential of Coker and Watts uses a well-defined prescription for the position of the fourth (not atom-centered) site on each molecule as a function of the positions of the atoms of that molecule. We shall use the site positions and charge values of the Coker and Watts model to define the necessary water parameters in the solute–water interaction potential.

For the solute–water interaction potential V^{SS}, we use a sum of atom–atom interactions, each of which has a short-range term V^{SR} and a coulombic term V^{C} such that

$$V^{SS} = V^{SR} + V^{C} \tag{1}$$

The short-range and long-range parts are modelled differently.

For the short-range interactions we use either a Lennard-Jones potential or an entirely repulsive potential, depending on the atom–atom interaction being considered. Thus, V^{SR} is given by

$$V^{SR} = \sum_{i=1}^{3n}\sum_{j=1}^{6} a_{\alpha\beta}e^{-b_{\alpha\beta}R_{ij}} - A_{\alpha\beta}R_{ij}^{-6} + B_{\alpha\beta}R_{ij}^{-12} \tag{2}$$

where n is the number of water molecules, so the sum over i runs over all water atoms, the sum over j runs over all solute atoms, and the indices α and β refer to the atom types of atoms i and j. For interactions between a solute chlorine atom and an atom in water, we set $A_{\alpha Cl}$ and $B_{\alpha Cl}$ equal to zero. The parameters $a_{\alpha Cl}$ and $b_{\alpha Cl}$ are taken from the chloride–water "simple" analytic potential of Kistenmacher et al.[48] For interactions between any solute methyl group atom and a water atom, $a_{\alpha\beta}$ and $b_{\alpha\beta}$ are set to zero, and $A_{\alpha\beta}$ and $B_{\alpha\beta}$ are taken from Clementi et al.[49] Clementi et al. use different values for $A_{\alpha\beta}$ and $B_{\alpha\beta}$, where α is a water hydrogen or oxygen, and β is a solute carbon or hydrogen, depending on the local environment of the carbon, which can be determined by the charge on the carbon. For example, for aliphatic carbon sites having only hydrogens and alkyl groups as substituents, Clementi et al. distinguish between (use different interaction parameters for) primary (average charge is −0.149 e), secondary (average charge is −0.373 e), and tertiary (average charge is −0.611 e) carbons. (We determined the average charge values from a study of amino acids by Clementi et al.[49]) Because the charge on the solute carbon in the present study varies from −0.183 e to −0.397 e along the reaction coordinate (see below), we use Clementi et al.'s interaction parameters for secondary carbons. For parameters for interactions of the solute hydrogens with the water, we use, for consistency, Clementi et al.'s values for a hydrogen attached to a secondary carbon. To be precise, we have listed all of the short-range interaction parameters in Table A1 in the Supplementary Material. We note that we chose the above mentioned parameter sets for the short-range solute–water interactions because they are compatible with a three-site atom-centered-site model for water, which, unlike a one-site short-range interaction model for water such as used in the TIP4P[50] and SPC[51] potentials, is unambiguous and realistic to extend to deformable water molecules. Also, the "simple" water model used by Clementi and co-workers[48] is very similar to the RWK2[42] water model that we use here. In particular, both models consider one site on each atom for short-range interactions. Although the model of Clementi and co-workers[48] has five charge sites and the RWK2[42] model has only three, two of these sites are placed on the hydrogen atoms as they are in the RWK2 model and one is placed 0.23 Å along the <HOH bisector, as compared to 0.26 Å along this bisector in the RWK2 model (for undeformed monomer). The remaining two charge sites of the model of Clementi and co-workers[48] are not expected to be very significant because they have charge values of less than 0.01 e. The values of the charge separation in the two models are also similar—the value of the negative charge site in the model of Clementi and co-workers[48] is 1.38 e as compared to a value of 1.2 e in the RWK2 model.

Table I. Values of the Parameters Used in Eq 4 To Define the Charge on the Carbon as a Function of r_c

parameter	value
A_C	0.214 e
C_C	−0.397 e
β_C	0.740 Å^{-2}

Table II. Values of the Solute Charges at the Gas-Phase Stationary Points[a]

	q_{Cl}	$q_{Cl'}$	q_C	q_H
$\mathcal{R}$	−1.000	−0.220	−0.397	0.206
$\mathcal{C}$	−0.946	−0.284	−0.341	0.190
‡	−0.627	−0.627	−0.183	0.146

[a] In units of e.

For the long-range part of the solute–water interaction, V^{C}, we use a sum of charge–charge interactions

$$V^{C} = \sum_{i=1}^{3n}\sum_{j=1}^{6} \frac{q_i^w q_j^s(r_c,r_{13})}{R_{ij}} \tag{3}$$

where the sum over i runs over all charge sites on the waters, three per water monomer, as defined in the RWK2 potential; the sum over j runs over all solute atoms; and R_{ij} is the distance between site i and site j. The charges q_i^w and q_j^s are defined as follows. For the charges at water sites, q_i^w, we use the values from the RWK2 potential; see ref 47. The solute charges, q_j^s, are a function of r_c, which is defined (as previously)[41] as the difference between the two carbon–chlorine bond lengths, and r_{13}, the chlorine–chlorine distance. For the chlorine charge values we use the charge values directly from surface S. For surface S, however, charge values are only defined for the two chlorines and for the methyl group as a single unit. Here we need the charges on the individual atoms. From a Mulliken population analysis of MP2/6-31G**[52] gas-phase wave functions at the three distinct stationary points, reactants ($\mathcal{R}$; $Cl^- + CH_3Cl$), complex ($\mathcal{C}$; $Cl^-\cdots CH_3Cl$), and saddle point (‡: $[Cl\text{–}CH_3\text{–}Cl]^-$),[53] we have a value for the charge on carbon as a function of r_c. We fit these charges as a function of r_c with the form

$$q_C = A_C e^{-\beta_C r_c^2} + C_C \tag{4}$$

where A_C and C_C are determined by the values of q_C at ‡ and $\mathcal{R}$, and β_C is then determined by the value of q_C at $\mathcal{C}$. The values of these parameters are given in Table I. We then find the charge on each hydrogen, q_H, by requiring that the sum of the charges on the individual methyl group atoms sum to the united methyl group charge, q_{Me}, of surface S, i.e.

$$q_H = \frac{1}{3}[q_{Me}(r_c,r_{13}) - q_C(r_c)] \tag{5}$$

(47) Coker, D. F.; Watts, R. O. *J. Phys. Chem.* **1987**, *91*, 2513.
(48) Kistenmacher, H.; Popkie, H.; Clementi, E. *J. Chem. Phys.* **1973**, *59*, 5842.
(49) Clementi, E.; Cavallone, F.; Scordamaglia, R. *J. Am. Chem. Soc.* **1977**, *99*, 5531.
(50) Jorgensen, W. L.; Chandrasekhar, J.; Madura, J. D.; Impey, R. W.; Klein, M. L. *J. Chem. Phys.* **1983**, *79*, 926.
(51) Berendsen, H. J. C.; Postma, J. P. M.; van Gunsteren, W. F.; Hermans, J. In *Intermolecular Forces*; Pullman, B., Ed.; Reidel: Dordrecht, Holland, 1981; p 331.
(52) We use the standard notation for ab initio electronic structure calculations. See, e.g.: Hehre, W. J.; Radom, L.; Schleyer, P. v. R.; Pople, J. A. *Ab Initio Molecular Orbital Theory*; John Wiley & Sons; New York, 1986.
(53) Tucker, S. C.; Truhlar, D. G. *J. Phys. Chem.* **1989**, *93*, 7356.

Table III. Internal Coordinates for $(H_2O)\cdot Cl^-$ Compared to Values for the Isolated Water Monomer

	$(H_2O)\cdot Cl^-$	H_2O model/experiment[a]
r_{ClH}	2.461 Å	
r_{H_dO}	0.971 Å	0.957 Å
r_{H_nO}	0.955 Å	0.957 Å
∠ClHO	161.4 deg	
∠HOH	100.9 deg	104.5 deg

[a] The model potential used here[43,46] was designed to reproduce the experimental geometry[54] of an isolated water molecule.

The values of q_{Cl}, $q_{Cl'}$, q_C, and q_H at $\mathcal{R}$, $\mathcal{C}$, and ‡ are given in Table II. We note that eq 14 assumes that the changes of charges along the reaction coordinate are unaffected by the solvent orientation. That is, it does not consider the polarization of the solute by the solvent. This approximation has been tested,[14,17] and it tends to underestimate the solute–solvent coupling. It would be interesting to see, in future work, whether our conclusions about nonequilibrium solvation are sensitive to this refinement of the potential energy function.

The full potential for reaction R2 with $n > 1$ is thus

$$V = V_S(\vec{x}) + V^{RWK2}(\vec{x};n) + V^W(\vec{x};n) + V^{SR}(\vec{x};n) + V^C(\vec{x};n) \quad (6)$$

where $\vec{x}$ is a vector giving the positions of all of the atoms of the system, the dimension of $\vec{x}$ being $3n + 18$, V_S is the potential of surface S which depends only on solute coordinates, and V^{RWK2}, V^W, V^{SR}, and V^C are as described above. For $n = 1$, we omit V^{RWK2} since it is not needed.

3. Stationary Points and Reaction Energetics

For $n = 1$ and 2, we have located and analyzed stationary points for reaction R2 which are microhydrated analogues of $\mathcal{R}$, $\mathcal{C}$, and ‡ of the unsolvated[41] reaction R1. Minima and saddle points were both found by a Newton–Raphson search over all coordinates. In this section we discuss the salient features of these stationary points. A complete set of Cartesian coordinates for all of these stationary points is given in the Supplementary Material of this paper. In section 3.1 we will discuss the microsolvated reactant for R2 with $n = 1$, $(H_2O)\cdot Cl^-$, and with $n = 2$, $(H_2O)_2\cdot Cl^-$. In section 3.2 we discuss the microsolvated complexes for $n = 1$ and $n = 2$, $(H_2O)_n\cdot Cl^-\cdots CH_3Cl$, and in section 3.3 we discuss the microsolvated transition states for $n = 1$ and $n = 2$, $(H_2O)_n\cdot[Cl\text{-}CH_3\text{-}Cl]^-$.

3.1. $(H_2O)_n\cdot Cl^-$. The structure of the $(H_2O)\cdot Cl^-$ ion is given in Figure 1a. It is qualitatively very similar to the structures found by Morokuma[6] in Hartree–Fock calculations with a 3-21G basis set and by Chandrasekhar et al.[8] from analytic fits to HF/6-31G* calculations. The most distinctive part of this structure is the apparent hydrogen bond between the chloride ion and the closer hydrogen, which we shall denote as H_d for donor. The Cl^-H_d distance is 2.46 Å, and the OH_d bond length is 0.971 Å, which is very similar to the donor OH bond length in the water dimer of Reimers and Watts,[44] 0.978 Å, as compared to a value in the isolated monomer of 0.957 Å.[43,46,54] The other OH bond length of 0.955 Å is also very similar to the corresponding OH bond length in the water dimer of Reimers and Watts,[44] 0.956 Å. We also see a 5% decrease in the HOH bond angle. The internal coordinates are given in Table III, along with values for the isolated water monomer for comparison.[43,46,54] For this configuration we find that the energy relative to the energy of infinitely separated Cl^- and H_2O, which is also (minus) the energy of microsolvation, is −9.4 kcal/mol. We also evaluate the enthalpy of microsolvation. In evaluating the thermodynamic energy, we treat vibrations by the harmonic, independent normal mode approximation. For the $(H_2O)\cdot Cl^-$ complex, we find an enthalpy of microsolvation of 8.7 kcal/mol, which, although qualitatively reasonable, is rather low compared to experimental values of 13.1 kcal/mol from one study and 14.7–14.9 kcal/mol from others.[55]

(54) Herzberg, G. *Molecular Spectra and Molecular Structure*; D. Van Nostrand Company: New York, 1966; Vol. III, p 585.

Table IV. Internal Coordinates for $(H_2O)_2\cdot Cl^-$: Isolated Water Dimer Geometries Are Given for Comparison[a]

	$(H_2O)_2\cdot Cl^-$	$(H_2O)_2$
$r_{OH_d}(A)$	0.973 Å	0.979 Å
$r_{OH_n}(A)$	0.966 Å	0.956 Å
$r_{OH_d}(B)$	0.976 Å	0.961 Å
$r_{OH_n}(B)$	0.959 Å	0.961 Å
$\angle HOH_d(A)$	100.1 deg	104.1 deg
$\angle HOH_d(B)$	101.7 deg	104.7 deg
$r_{H_dO}(A,B)$	1.85 Å	1.76 Å
$r_{H_dCl}(B)$	2.44 Å	
$r_{H_nCl}(A)$	2.74 Å	
dihedral angle $\angle H_n(A)O(A)O(B)H_d(B)$ = 13.6 deg		

[a] From the potential model used here, ref 47. A is defined as the water having the donor hydrogen of the water–water hydrogen bond, H_d are donor hydrogens, H_n are not (see Figure 1b).

For the $(H_2O)_2\cdot Cl^-$ complex, we find the energy relative to infinitely separated molecules (ions), i.e., $H_2O + H_2O + Cl^-$, is −21.3 kcal/mol. The energy change for addition of the second water to the $(H_2O)\cdot Cl^-$ complex is therefore −11.9 kcal/mol. The enthalpy change for this process is −9.8 kcal/mol, compared with experimental values which range from −12.6 to −13.0 kcal/mol.[55] In our model, the energy (and enthalpy) change for adding the second water is greater than that for adding the first, because we get an additional contribution from the water–water interaction. (Although this trend is not in agreement with experiment[55] for microhydration of Cl^-, a similar effect *has* been found[56] for microsolvation of transition-metal atomic ions.) If the chloride–water interactions in our potential model were stronger, the water–water interaction energy would not be as large a percentage of the energy change for the addition of the second water molecule, and we would reproduce the experimental result that the enthalpy change for adding the second water is less than that for adding the first. We conclude that although the potential yields microhydration enthalpies accurate to within a few kcal/mol, the chloride–water interaction is probably quantitatively too weak.

This explanation is supported by the structure for $(H_2O)_2\cdot Cl^-$ which has a hydrogen bond between water B and hydrogen $H_d(A)$ on water A, which points toward water B in Figure 1b. A summary of the internal coordinates is given in Table IV, along with values for the water dimer[47] for comparison. As evidence that the hydrogen–water interaction is a hydrogen bond, we note that the distance between $H_d(A)$ and the oxygen of water B is 1.85 Å as compared to a hydrogen bond length of 1.77 Å in the water dimer of Reimers and Watts.[44] Also, the water A OH_d bond distance of 0.973 Å is correctly lengthened from the monomer value of 0.957 Å. Figure 1b also shows one hydrogen on each water pointing (roughly) toward the chloride ion. For water B, the OH bond length for this hydrogen is 0.976 Å, and the distance to the chloride from this hydrogen is 2.44 Å. These distances indicate that this hydrogen forms a hydrogen bond with the chloride ion, and we refer to it as $H_d(B)$ in Table IV. The hydrogen on water B which is barely seen in Figure 1b is clearly non-hydrogen-bonding, and we denote it $H_n(B)$ in Table IV. Finally, the remaining hydrogen on water A, which points roughly toward the chloride ion, appears to form a partial hydrogen bond with the chloride (however, we label it $H_n(A)$ in Table IV to distinguish it from $H_d(A)$ which is the donor hydrogen for the water–water hydrogen bond). This partial H bond character is illustrated by an intermediate OH bond length of 0.966 Å (compared to the length of $OH_d(B)$ of 0.976 Å and $OH_n(B)$ of 0.959 Å) and an intermediate hydrogen chloride distance of 2.74 Å (compared to the $H_d(B)$–Cl distance of 2.44 Å).

In Table V, we give harmonic frequencies for the two reactant structures. For comparison, we also list harmonic frequencies for the water monomer and water dimer, both from experiment[54,57,58]

(55) Keesee, R. G.; Castleman, A. W., Jr. *J. Phys. Chem. Ref. Data* **1986**, *15*, 1018.
(56) Marinelli, P. J.; Squires, R. R. *J. Am. Chem. Soc.* **1989**, *111*, 410.
(57) Dyke, T. R.; Mack, K. M.; Muenter, J. S. *J. Chem. Phys.* **1977**, *66*, 498.

Table V. Harmonic Frequencies at the Minima: Gas-Phase Results (from ref 41) and Water Monomer and Dimer Frequencies Are Included for Comparison

H_2O		$(H_2O)_2$								
exp[a]	model	exp[b]	model	$(H_2O)\cdot Cl^-$	$(H_2O)_2\cdot Cl^-$	$\mathscr{C}$	$(H_2O)\cdot\mathscr{C}$	$(H_2O)_2\cdot\mathscr{C}$	source[c]	description
							d	*d*	S/T	$(H_2O)_n$ free rotor
							9	12	S/T	H_2O–Cl–CH_3Cl bend
							10	14	S/T	H_2O–Cl–CH_3Cl bend
		d	115[e]		80			63	D/T	H_2O torsion around OH_d(A) bond
						68	66	66	C/T	Cl–C–Cl bend
						68	67	67	C/T	Cl–C–Cl bend
						113	86	88	C/T	Cl–CH_3Cl stretch
				132	135		136	139	S/T	Cl–$(H_2O)_n$ stretch
		d	169		179			186	D/T	H_2–O–H_2O(A) bend
		d	219		254			247	D/T	H_2O(B) torsion around C_{2v} axis
				269	266		258	267	S/T	Cl–H_dO bend
		150	272		457			439	D/T	H_2O–H_2O stretch
		d	483		486			477	D/T	H_d–O(A)–O(B) in plane bend
				603	728		574	715	S/T	H_2–O–Cl bend
						698	706	709	C/M	CH_3–Cl stretch
		d	782		787			785	D/T	H_d–O(A)–O(B) out-of-plane bend
						970	977	982	C/M	CH_3 rock
						970	977	983	C/M	CH_3 rock
						1305	1316	1324	C/M	CH_3 umbrella
						1429	1431	1432	C/M	CH_3 deformation
						1429	1431	1433	C/M	CH_3 deformation
1595	1639	1593	1620	1758	1717		1747	1706	D/M	H–O–H bend(B)
		1611	1682		1814			1804	D/M	H–O–H bend(A)
						3035	3027	3021	C/M	C–H stretch
						3155	3146	3139	C/M	C–H stretch
						3155	3146	3140	C/M	C–H stretch
		3550	3527		3586			3577	D/M	O–H_d stretch
3657	3817	3627	3784	3681	3646		3696	3657	D/M	O–H stretch
		3699	3887		3776			3790	D/M	O–H stretch
3756	3922	3715	3888	3919	3875		3916	3873	D/M	O–H_n stretch

[a] Reference 54. [b] References 57 and 58. [c] The source of each mode is categorized by one of the following designations: C/T, a transient mode of the complex, i.e., one which goes to zero when Cl^- is infinitely far from CH_3Cl; C/M, a mode of the complex which also appears in CH_3Cl; D/T, a transient mode of the water dimer, i.e., one which goes to zero for one H_2O infinitely far from the other H_2O; D/M, a mode of the water dimer which also appears in the water monomer; S/T, a transient mode of any solvated species, i.e., one which goes to zero when the solvent is infinitely far from the solute. [d] Not available. [e] Frequencies are in cm^{-1}.

Table VI. Internal Coordinates for $(H_2O)\cdot Cl^-\cdots CH_3Cl$

r_{ClH_d} = 2.50 Å	∠HOH = 101.2 deg
r_{OH_d} = 0.970 Å	∠ClH_dO = 162.8 deg
r_{OH_n} = 0.955 Å	∠ClCCl = 179.4 deg
$r_{\overrightarrow{CCl}}$ = 3.20 Å	

Table VII. Internal Coordinates for $(H_2O)_2\cdot Cl^-\cdots CH_3Cl$[a]

r_{OH_d}(A) = 0.974 Å	∠HOH_d(A) = 100.4 deg
r_{OH_n}(A) = 0.965 Å	∠HOH_d(B) = 102.0 deg
r_{OH_d}(B) = 0.974 Å	
r_{OH_n}(B) = 0.959 Å	
r_{H_dO}(A,B) = 1.84 Å	
r_{HCl}(A) = 2.80 Å	
r_{H_dCl}(B) = 2.47 Å	
$r_{\overrightarrow{CCl}}$ = 3.26 Å	

[a] Notation is the same as in Table IV.

and from the potential model.[47]

3.2. $(H_2O)_n\cdot Cl^-\cdots CH_3Cl$. We find the energy of the n = 1 complex relative to the energy of $H_2O + CH_3Cl + Cl^-$ is −19.5 kcal/mol. The energy of microsolvation (n = 1) of the gas-phase complex is then 8.5 kcal/mol, slightly less than the microsolvation energy of a lone chloride ion, and the energy difference between the reactants of R2 with n = 1 and the complex of R2 with n = 1 is −10.1 kcal/mol. Figure 2 is a schematic diagram of the reaction energetics for reactions R1, R2 with n = 1 and R2 with n = 2.

The n = 1 complex is shown in Figure 1c. We list relevant internal coordinates in Table VI. In this structure, we see that the water still bonds primarily to the more negatively charged chlorine, with a geometry similar to the $(H_2O)\cdot Cl^-$ geometry, although the water is somewhat rotated and the HOH angle has been increased slightly. The solute geometry no longer retains C_{3v} symmetry, although all deviations from the gas-phase complex[41] are of the order of 0.5 deg for angles and 0.01 Å for bond lengths, except for the longer CCl bond, $r_{\overrightarrow{CCl}}$, which is increased by 0.06 to 3.20 Å.

The most interesting aspect of this complex is that there is virtually no barrier to rotation of the water molecule around the solute "C_{3v} symmetry axis". (Although the C_{3v} symmetry axis is no longer truly defined, it is still a useful construct, since the deviations of the solute from C_{3v} symmetry are so small.) The barrier to this rotation is less than 0.0005 kcal/mol. Finally, we note that Chandrasekhar et al.[8] and Morokuma[6] also predict an end-on water structure for the one water complex.

In Figure 1d we show the structure for the complex with two waters, $(H_2O)_2\cdot Cl^-\cdots CH_3Cl$, and in Table VII we give some of the relevant internal coordinates. As in the complex with one water, both waters interact almost entirely with the far, more highly charged chlorine; their interaction with the MeCl is minimal, and the MeCl shows only very minor deviations from C_{3v} symmetry. In this case, there is a significant water–water interaction, and the barrier for rotation of the water dimer, as a unit, around the solute "C_{3v} symmetry axis" is virtually nonexistent, at ~0.003 kcal/mol. Note first that the longer CCl bond has extended further, to 3.26 Å, which is 0.12 Å longer than in the gas-phase complex. The water–water–chlorine arrangement resembles that of $(H_2O)_2\cdot Cl^-$, and we use the notation developed in the discussion of this structure: H_d(A), H_n(A), H_d(B), and H_n(B); it has one water–water hydrogen bond, H_d(A)–O(B), which has a "bond" distance of 1.84 Å and two fairly strong hydrogen chlorine interactions, H_d(B)–Cl and H_n(A)–Cl, which have internuclear distances of 2.47 and 2.80 Å, respectively. The intramolecular OH bond lengths reflect the degree of hydrogen bonding for each H as seen in the previous structures. Finally, we again see that the HOH angles are smaller than in the un-

(58) Bentwood, R. M.; Barnes, A. J.; Orville-Thomas, W. J. *J. Mol. Spectrosc.* **1980**, *84*, 391.

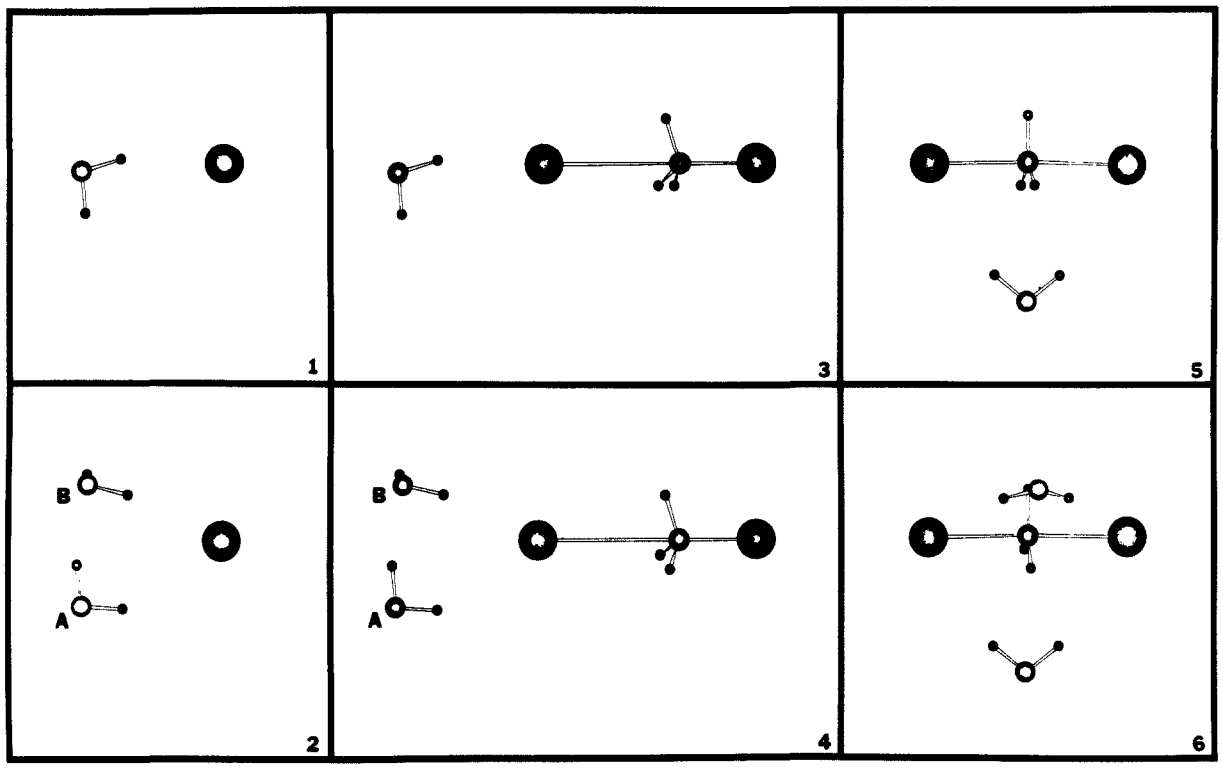

Figure 1. Illustrations of the stationary points for the reaction R2 with $n = 1$ and $n = 2$. Parts a–f, which are labeled 1–6, respectively, are as follows: (a) $(H_2O)\cdot Cl^-$, all four atoms lie in a plane; (b) $(H_2O)_2\cdot Cl^-$; (c) the complex $(H_2O)\cdot Cl^-\cdots CH_3Cl$, the water molecule lies in the same plane as both chlorines, the carbon, and one methyl hydrogen; (d) the complex $(H_2O)_2\cdot Cl^-\cdots CH_3Cl$; (e) the saddle point $(H_2O)\cdot[Cl\text{–}CH_3\text{–}Cl]^-$, the water molecule lies in the same plane as both chlorines, the carbon, and the one methyl hydrogen; it falls midway between the other two methyl hydrogens; (f) the saddle point $(H_2O)_2\cdot[Cl\text{–}CH_3\text{–}Cl]^-$, each water is located symmetrically with respect to the chlorines; i.e., the oxygens are in the methyl plane; they are located equal distances from the carbon; this structure has a C_{2v} symmetry axis defined by the carbon and the methyl hydrogen which points out from the plane of the figure.

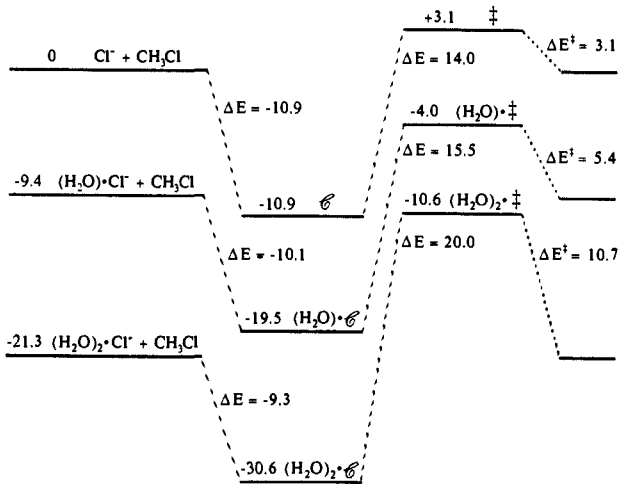

Figure 2. Reaction energetics, on an energy scale (kcal/mol) having the zero of energy at infinitely separated $H_2O + H_2O + Cl^- + CH_3Cl$, for reaction R2 with $n = 0$, 1, and 2. For all reactions the complex on the product side has been omitted from the diagram.

perturbed monomer. We note that Morokuma[6] found, for the two-water complex, that both waters interacted most strongly with the more negatively charged chlorine. In the structure found by Morokuma, the two waters are further apart than in the structure found with the present model and do not appear (from the published stick diagram) to be in the proper orientation to have a water–water hydrogen bond between them.

The energy of this two-water complex relative to the energy of $2H_2O + Cl^- + CH_3Cl$ is −30.6 kcal/mol, yielding an energy of microsolvation for $n = 2$ of 19.7 kcal/mol. The energy of microsolvation for the $n = 1$ complex going to the $n = 2$ complex is 11.1 kcal/mol; see Figure 2. Again, the larger energy gain associated with adding the second water is due to the water–water interaction. Finally, in Table V we give the frequencies of the complex with one water, the complex with two waters and, for comparison, the gas-phase complex. A useful comparison can also be made with the previously mentioned frequencies listed in that table, since water–water and chloride ion–water type interactions dominate the interaction spectrum. The correlation of frequencies from the various compounds is fairly straightforward.

Table VIII. Internal Coordinates for $H_2O\cdot[Cl\text{–}CH_3\text{–}Cl]^-$ at the Saddle Point

$r_{OH} = 0.962$ Å	∠HOH = 103.1 deg
$r_{CCl} = 2.296$ Å	∠ClCCl = 177.7 deg
$r_{CO} = 3.17$ Å	
$r_{HCl} = 2.96$ Å	
$r_{H_{Me}O} = 2.80$ Å	

3.3. $(H_2O)_n\cdot[Cl\text{–}CH_3\text{–}Cl]^-$. Now we consider the microsolvated saddle point structures. We start with the saddle point for reaction R2 with $n = 1$. The optimized structure is given in Figure 1e. The water is located symmetrically between the two chlorines and between two of the hydrogens to yield a transition state with C_{2v} symmetry. Each water hydrogen forms a partial hydrogen bond with the nearest chlorine, as suggested by an H–Cl bond length of a moderate 2.96 Å and a water OH distance having an intermediate value of 0.962 Å. The methyl group hydrogens interact only weakly with the water oxygen, with an internuclear distance of 2.80 Å. The solute is noticeably perturbed from C_{3v} symmetry, with the chlorines bent toward the water hydrogens, and the methyl hydrogens bent away. The ClCCl angle is reduced from linear by 2.3 deg; the HCH angle is increased from 120 deg by 0.9 deg. Relevant internal coordinates are given in Table VIII. Chadrasekhar et al.[8] found quite a different structure with their model. They found the water to hang off of the end of the solute molecule near one of the chlorines, similar to the structure at the complex. We found no evidence of a similar, asymmetric stationary point for our model. Morokuma[6] found structures of both types. These differences should be expected in this kind of study

Table IX. Internal Coordinates for $(H_2O)_2{\cdot}[Cl{-}CH_3{-}Cl]^-$ at the Saddle Point

r_{OH}(A or B) = 0.962 Å	∠HOH (A or B) = 103.3 deg
r_{CCl} = 2.291 Å	$\angle H_{Me}CH_{Me}$ (surrounding water A or B) = 120.5 deg
r_{ClH} = 2.99 Å	∠ClCCl = 177.6 deg

because there often exist only small barriers to reorientation of solvent molecules around a solute, and as a result small energy variances between different models of the potential interactions may lead to stationary points which differ in a qualitative fashion.

Energetically (see Figure 2) we find the n = 1 saddle point is 4.0 kcal/mol lower in energy than $H_2O + Cl^- + CH_3Cl$ or 7.1 kcal/mol lower than the gas-phase saddle point. The energy barrier relative to the reactants of R2 with n = 1 is 5.4 kcal/mol.

The structure of the saddle point for reaction R2 with n = 2 is very similar to the n = 1 saddle point; it is pictured in Figure 1f. Note that it has C_{2v} symmetry; the geometry is given in Table IX. The energy of the n = 2 saddle point is −10.6 kcal/mol relative to $H_2O + H_2O + Cl^- + CH_3Cl$, or 10.7 kcal/mol relative to the reactants of R2 for n = 2, or −6.6 kcal/mol relative to the n = 1 saddle point. The saddle point configuration has no water–water hydrogen bond; consequently the addition of the second water gives a smaller energy change than did the addition of the first. Considering Figure 2 we see, just from n = 0, n = 1, and n = 2, that the reaction energetics are tending toward those of the aqueous phase reaction. For n = 2, as compared to n = 0, the well has become more shallow by 1.5 kcal/mol, and the barrier height has increased by 7.6 kcal/mol. The n = 2 barrier height of 10.7 kcal/mol is 40% of the solution phase barrier of 26.6 kcal/mol.[59] This eventual point of convergence, however, requires many more waters. E.g., Kong and Jhon[11] found, by using ab initio calculations combined with a simple model for the water potential, that it requires about 50 water molecules to converge the calculated barrier height for reaction R2. Finally, in Table X, we list the frequencies for the saddle points for the reaction R2 with n = 0, n = 1, and n = 2. Of special note is the imaginary frequency, which corresponds to the inverse barrier frequency at the saddle point. This frequency increases by 115 cm^{-1} upon addition of one water and by an additional 85 cm^{-1} upon the addition of the second water molecule.

Table X. Harmonic Frequencies for the Saddle Points for Reaction R2 with n = 0, 1, and 2[c]

H_2O	‡ (n = 0)	‡ (n = 1)	‡ (n = 2)	source[a]	description[b]
	469i	584i	669i	C/T	asymmetric stretch
			22	S/T	H_2O–C–H_2O bend
			43	S/T	H_2O in plane rock (o)
		47	44	S/T	H_2O in plane rock (c)
			86	S/T	H_2O–$ClCH_3Cl$ stretch (o)
		92	91	S/T	H_2O–$ClCH_3Cl$ stretch (c)
		113	153	S/T	$ClCH_3Cl$ twist around Cl–Cl axis
	206	206	205	C/T	Cl–C–Cl bend
	206	211	219	C/T	Cl–C–Cl bend
	220	231	235	C/M	symmetric stretch
			315	S/T	H_2O torsion around C–O axis (c)
		328	325	S/T	H_2O torsion around C–O axis (o)
			357	S/T	CH_3–H–O bend (c)
		363	361	S/T	CH_3–H–O bend (o)
			395	S/T	CH_3–O–H_2 bend (c)
		422	413	S/T	CH_3–O–H_2 bend (o)
	947	948	950	C/M	CH_3 rock
	947	950	952	C/M	CH_3 rock
	1021	1023	1025	C/M	CH_3 umbrella
	1381	1384	1389	C/M	CH_3 deformation
	1381	1388	1391	C/M	CH_3 deformation
1639		1701	1689	W/M	H–O–H bend
			1699	W/M	H–O–H bend
	3106	3105	3104	C/M	C–H stretch
	3309	3307	3307	C/M	C–H stretch
	3309	3309	3308	C/M	C–H stretch
3817		3751	3754	W/M	symmetric stretch
			3756	W/M	symmetric stretch
3922		3854	3856	W/M	asymmetric stretch
			3860	W/M	asymmetric stretch

[a] Source designations are the same as those used in Table V, except for the additional designator W/M which indicates a mode which appears in an isolated water monomer. [b] For n = 2, each pair of S/T modes having the same description are mixed to form a concerted/opposed pair. Each description is followed by (c) or (o) to designate whether in the n = 2 case it is the concerted or the opposed mode. [c] Frequencies are in cm^{-1}.

4. Theory

The approximation that solvation of transition states may be treated by equilibrium statistical thermodynamics underlies all standard treatments of solvation effects on reaction rates.[1-3,59] In addition, most treatments make the further assumption that the solvent remains in equilibrium with the solute throughout the reactive process and, consequently, that only static solvent effects are important. However, the mechanics of combining equilibrium solvation with transition-state theory (TST) requires further study.[12,16,19,34,36-40] Thus, in this section, we discuss new methods for applying conventional and generalized[30-32,35] TST in the context of equilibrium solvation and nonequilibrium solvation. We begin, in section 4.1, by presenting variational transition-state theory with an extended notation which allows us, in section 4.2, to precisely define the nonequilibrium–solvation TST method and two distinct equilibrium–solvation TST methods. Details of these methods are given in section 5, and in section 6 we apply them to the simple cluster reaction R2.

4.1. Variational Transition-State Theory. Variational transition-state theory is only useful if, even when the search over generalized transition states is restricted enough to be practical, we can find a variational transition state which acts as a good dynamical bottleneck to reaction. Once we have defined a generalized transition state—taken here as a hyperplane in coordinate space—we assume that any trajectory that crosses this hyperplane in the direction from reactants to products will never return to reactants. As discussed elsewhere,[30,32,35] this formulation of generalized transition-state theory for hyperplanes leads to the following expression for a bimolecular rate constant in terms of free energies of activation:

$$k^{GT} = \frac{\tilde{k}T}{h} K^0 e^{-\Delta G_T^{GT,0}(s,\hat{g})/RT} \qquad (7)$$

where k^{GT} is the generalized TST rate constant, $\tilde{k}$ is the Boltzmann constant, h is Planck's constant, T is temperature, K^0 is the reciprocal of the standard state concentration, s and $\hat{g}$ specify the generalized transition state (see below), $\Delta G_T^{GT,0}$ is the standard state generalized free energy of activation for the generalized transition state defined by s and $\hat{g}$, and R is the ideal gas constant. In all cases discussed in this article, vibrations are quantized in the calculation of $\Delta G_T^{GT,0}(s,\hat{g})$.

A generalized transition state in $3N$-dimensional space is a $(3N-1)$-dimensional entity, restricted in this work to be a hyperplane. The hyperplane is specified by two values: the distance s along the curvilinear minimum energy path (MEP) at which it (the MEP) crosses the hyperplane and the unit vector $\hat{g}$ normal to the surface. The "missing degree of freedom" of the generalized transition state is a Cartesian coordinate orthogonal to the hyperplane. This is called[35] the local reaction coordinate ($\hat{g}$).

The generalized free energy of activation is the free energy change between the reactants and a generalized transition state "species", where this "species" does not include the local reaction coordinate. Because, for each prescription we employ for $\hat{g}$, we define a series of generalized transition states along the reaction path, we can evaluate a generalized free energy of activation *curve*, $\Delta G_T^{GT,0}(s,\hat{g})$, which is parameterized by s as defined above. In order to evaluate the variational transition-state rate constant,

(59) Albery, W. J.; Kreevoy, M. M. *Adv. Phys. Org. Chem.* **1978**, *16*, 87.

the variationally best generalized transition state in the series considered must be chosen. At a fixed temperature, the best generalized transition-state species is the one which yields the maximum value of the free energy of activation curve,[30-32,35] and the point at which this best generalized transition state intersects the reaction path will be called s_*^{CVT}. Throughout this paper, we shall refer to the specific generalized transition state defined by s_*^{CVT} for a given prescription for $\hat{g}$ as a "variational transition state".

It is useful to introduce another formulation[30-32,35] of generalized transition-state theory which is equivalent to eq 7, in particular

$$k^{GT} = \frac{\tilde{k}T}{h} \frac{Q^{GT}(T,s,\hat{g})}{\Phi^R(T)} e^{-V_{min}(s,\hat{g})/\tilde{k}T} \quad (8)$$

In eq 8, $\Phi^R(T)$ is the reactants partition function per unit volume. The quantities which are dependent on the choice of generalized transition-state hyperplane are Q^{GT}, the quasi-partition function of the generalized transition-state species, and V_{min}, its zero of energy. The quantity Q^{GT} is referred to as a quasi-partition function because it is the partition function for a fictitious species which has one degree of freedom, the local reaction coordinate $\hat{g}$, fixed.

For gas-phase reactions without solvation or microsolvation, it has been found that the minimum energy path (MEP), defined[32] as the path of steepest descents in mass-weighted or mass-scaled[60,61] coordinates connecting the saddle point with reactants, is a good coordinate to use both as the reaction path to parameterize a sequence of possible generalized transition states and as the local reaction coordinate to determine the orientations of these generalized transition states. If we do this, the set of possible generalized transition states are orthogonal to the MEP, $\hat{g}$ is the local tangent to the MEP, and $V_{min}(s)$ is the value of the potential on the MEP at a distance s (along the MEP) from the saddle point. Very good estimates of gas-phase rate constants may be obtained by using the variational transition state from this set.[1,31,35,62] Thus the MEP provides one practical prescription for choosing a variational transition state and applying variational TST. We note that conventional TST can be seen as a special case of this prescription, one in which the transition state is chosen to be at the saddle point ($s = 0$), rather than at the variationally optimized position, and is orthogonal to the MEP (at $s = 0$ the MEP is tangent to the eigenvector associated with the saddle point imaginary frequency).

The final estimate of the rate constant is $\kappa(T)$ times the minimized value of $k^{GT}(T,s_*^{CVT})$, where $\kappa(T)$ is a transmission coefficient that accounts for quantum mechanical effects on motion along the reaction coordinate. In this section, however, we are not concerned with these quantal effects.

4.2. Equilibrium vs Nonequilibrium Solvation. One cannot apply the above prescription without modification to reactions in bulk solution, because it is computationally impossible to treat all degrees of freedom of the system, solute plus solvent, explicitly, except by classical mechanical simulation approximations, which do not include the important effects of quantized energy levels which are included in eqs 7 and 8. One way to treat bulk solvation effects on kinetics, while also treating primary system vibrations as quantized, is to conceptually partition the system into two parts—a reacting part (often just the solute) called the primary system, for which all degrees of freedom are treated explicitly, and a bath, which is treated in a reduced dimensionality. The simplest way to apply TST to a system in which such a primary system–bath separation has been made is to assume that the bath makes only energetic contributions to the reaction process, i.e., that bath coordinates and variations in the primary system MEP due to the effect of the bath are unimportant. Thus, TST is applied by using the primary system MEP, in the absence of the bath, to define the local reaction coordinate but including the bath contribution to the free energy when evaluating the rate constant.[3,39] Physically this prescription corresponds to the equilibrium solvation assumption, the assumption that the bath molecules adjust statistically to motions of the primary system, i.e., that the bath always remains in equilibrium with the primary system. We note that changes in the reaction rate from gas phase to solution which are due to this kind of bath contribution to the free energy are called static solvation effects, while those changes in the reaction rate which are due to a breakdown of the equilibrium solvation assumption are called nonequilibrium or dynamic solvation effects. To test the assumption of equilibrium solvation, in the present article we apply it not to a bulk-solvated reaction but to a microsolvated one for which we can also perform the calculation without a system–bath separation.

For our tests of the equilibrium solvation model, we will use the simplest primary system–bath separation, which is to take the solute as the primary system. The first step is to find the equilibrium solvation reaction path. The solute coordinates on the equilibrium solvation path have, by definition, the same values as on the gas-phase MEP. The solvent coordinates must then be optimized (to find the minimum energy configuration), for fixed solute coordinates, at each point on this reaction path. The sequence of geometries obtained this way is the equilibrium solvation path (ESP).

In order to evaluate generalized transition-state theory rate constants, however, we need to know the generalized free energy of activation. As for gas-phase calculations, we will find a good generalized transition state by maximizing the free energy of activation for a one-parameter series of generalized transition states. Our gas-phase prescription, however, cannot be used without modification for the equilibrium solvation model. In a gas-phase calculation or a nonequilibrium solvation calculation, we define the generalized transition state at each point on the MEP by making it orthogonal to the MEP, and this guarantees that V_{min} in the generalized transition state will be at the point where the MEP and the generalized transition state (hyperplane) intersect. In an equilibrium solvation calculation, we cannot simultaneously make the generalized transition state orthogonal to the equilibrium solvation path (ESP) and make the ESP be the point of minimum potential energy in the generalized transition state, because the gradient of the potential does *not* point along the ESP (i.e., the gradient at a given point on the path is not parallel to the tangent to the path at that point).

There are, however, at least two reasonably straightforward choices for dividing surface orientation. The first choice is to make the generalized transition state orthogonal to the gradient at each point on the ESP, i.e., to use the local gradient to define the local reaction coordinate at each point. We note that the local gradient vector, at each point on the ESP, only has nonzero components for the solute coordinates, because, by definition, all of the solvent coordinates are at a stationary point (a minimum) relative to the fixed solute coordinates at each point on the ESP. (Of course this does not contradict the fact that the ESP has a solvent component since we are distinguishing between the gradient on the ESP and ESP itself.) With this choice of dividing surface, the ESP will intersect each generalized transition-state hyperplane at the point of minimum potential energy in that generalized transition state. The second choice for generalized transition-state orientation is to make the hyperplane orthogonal to the *gas-phase* gradient, i.e., the gradient of the solute potential in the absence of the solvent interactions at each point on the ESP. One effect of this second choice is that the local reaction coordinate is restricted to the solute degrees of freedom, since these are the coordinates of the gas-phase MEP. We will employ both of these choices for full calculations. These two approaches will be called the "solvent influenced" local reaction coordinate method and the "gas-phase" local reaction coordinate method, respectively.

A third possibility would be to take the hyperplane locally orthogonal to the ESP, but this requires more extensive calculations and was not pursued. However, it might be interesting to study in future work.

Finally, we note that "conventional transition-state theory" does not appear to have an unambiguous definition in the context of

(60) Garrett, B. C.; Truhlar, D. G. *J. Phys. Chem.* **1979**, *83*, 1079.
(61) Isaacson, A. D.; Truhlar, D. G. *J. Chem. Phys.* **1982**, *76*, 1380.
(62) Truhlar, D. G.; Garrett, B. C. *Annu. Rev. Phys. Chem.* **1984**, *35*, 159; *J. Chim. Phys.* **1987**, *84*, 365.

equilibrium solvation, because there is no true saddle point (where all first derivatives are zero) on the ESP, and, in addition, the point on the ESP which corresponds to the gas-phase saddle point will not necessarily be the point of highest potential energy on the ESP, although it may often be. Even if the gas-phase saddle point did correspond to the highest point on the ESP, one would still have to ask whether the "conventional" transition state should be placed orthogonal to the imaginary frequency of the full system, to the imaginary frequency of the gas-phase saddle point, or to the ESP itself.

With these definitions we can address the question of equilibrium vs nonequilibrium solvation. Physically, equilibrium solvation might be expected to be a poor assumption when the time scale for motion along the reaction path is much faster than the time scale for solvent reorganization, but the ratio of these time scales is not usually clear. If the reaction path time scale were much faster than the solvent reorganization one, the reactivity of a given trajectory would be largely dependent upon the initial configuration of the solvent, and, since every trajectory which crosses the generalized transition-state hyperplane is assumed to be reactive, a generalized transition state which does not account for this configuration will overcount the number of reactive trajectories. This effect is referred to as solvent-induced recrossing (of the generalized transition state). It is sometimes assumed that recrossing of the generalized transition state in an equilibrium solvation calculation is evidence of solvent-induced recrossing,[12,13,21] i.e., a breakdown of the equilibrium solvation assumption. However, in order to be sure of this, one must ascertain whether the definition of generalized transition state that is used provides a good dynamical bottleneck for the equilibrium solvation reaction; if this proves true, then additional recrossing effects may be attributable to solvent-induced recrossing. Thus, it is important to distinguish recrossing effects due to a poor choice of dynamical bottleneck for the equilibrium solvation reaction from the breakdown of that assumption itself. We will use variational transition-state theory to accomplish this.

5. Methods

In order to distinguish between different possible causes of recrossing effects we consider the simplest case where a system–"bath" separation can be made—that of a reacting solute in the presence of one solvent molecule—and we evaluate the variational TST rate constant by a number of different methods. We consider first a nonequilibrium solvation calculation, where we make no system–bath separation, we treat all of the coordinates of the system explicitly, and we use our gas-phase prescription[30-32,35] for choosing the variational transition state. We then consider two calculations based on the ESP. The first of these calculations takes the local reaction coordinate to be the gradient of the solvent-influenced solute, i.e., to be the gradient of the full potential surface at each point on the ESP, whereas the second defines the local reaction coordinate to be the gradient of the unperturbed solute, i.e., the gas-phase gradient evaluated in the absence of the solvent. In all three methods with use temperature-dependent variational transition states. For the nonequilibrium solvation calculation this is the standard canonical variational TST (CVT) prescription.[30-32,35] Finally, we also perform nonequilibrium solvation calculations for the case of two solvent molecules, because we are also interested in the trends in cluster reaction rates as the number of water molecules is increased incrementally.

For the nonequilibrium solvation calculations, with $n = 1$ and $n = 2$, we consider both conventional transition-state theory and CVT.[30-32,35] As in our gas-phase study of this reaction,[41] we consider tunneling corrections to the CVT rate constants calculated by the minimum energy path semiclassical adiabatic ground-state method (MEPSAG)[32,35,63] and by the small curvature semiclassical adiabatic ground-state method (SCSAG).[64,65] The latter is the most reliable of the methods considered here.

For all of the calculations, we used the POLYRATE computer program (version 1.5),[66] although for the equilibrium solvation calculations we required the modifications discussed below. For all calculations discussed we calculated the vibrational partition functions by the quantum mechanical harmonic independent-normal-mode approximation,[32] and we calculated the rotational partition functions classically. We use the reduced mass $\mu = 1$ amu in all cases for mass scaling[32] the coordinates.

For the equilibrium solvation calculations, we evaluated the ESP from the gas-phase MEP, by minimizing the solvent coordinates for fixed solute coordinates at a grid of points (defined by s) on the gas phase MEP. We parameterize the free energy of activation curves for the equilibrium solvation calculations by the value of the point s on the gas-phase MEP. The ESP itself then consists of the combination of the solute coordinates and the optimized solvent coordinates at each point s.

For the solvent-influenced local reaction coordinate method, the partition functions of the generalized transition state are defined in the usual fashion;[32] to evaluate the vibrational partition functions on the reaction path the full local gradient at each point s (in this case on the ESP) is projected out of the vibrational subspace in order to determine the frequency spectrum in the generalized-transition-state hyperplane. In the solvent-influenced local reaction coordinate method, a projection operator is also used at $s = 0$ (which corresponds to the gas-phase saddle point), because this is not a stationary point on the ESP. The rotational partition functions are based on the moment of inertia for the geometry of the solute plus solvent on the ESP.

For the gas-phase local reaction coordinate equilibrium solvation calculation, we again project a degree of freedom from the vibrational subspace to determine the generalized-transition-state frequency spectrum at each value of s; but in this case we use the gradient of the gas-phase MEP at this point, determined with the water and water–solute potentials set to zero. At $s = 0$ we remove the vector associated with the gas-phase imaginary frequency, which is tangent to the gas-phase MEP at this point, since the gas-phase gradient is zero at this point. The rotational partition functions are treated as in the solvent-influenced local reaction coordinate method.

In the nonequilibrium solvation calculations and in the solvent-influenced local reaction coordinate method, removing the local reaction coordinate from the generalized transition state (at some value of s) guarantees that all the degrees of freedom remaining in the generalized transition state will be at a stationary point at the point where they intersect the reaction path, and V_{min} in eq 8 is just the value of the full potential energy surface at s on the path. Because we do not remove the full gradient of the potential energy function from the dividing surface in the gas-phase local reaction coordinate method, there may be a nonzero gradient in the generalized transition-state theory hyperplane at the point where it intersects the ESP, and we must find the correction, δV, to the value of the potential energy function on the ESP, V^{ESP}, in order to evaluate V_{min} in eq 8 by

$$V_{min} = V^{ESP}(s) - \delta V(s) \tag{9}$$

This is carried out in the harmonic independent normal mode approximation.

6. Results

6.1. Effect of Microsolvation on Reaction Dynamics. For the reaction rate calculations presented in this section, we do not assume that the water molecules stay in equilibrium with the solute during the course of the reaction, and hence we refer to these results as nonequilibrium solvation rate constants. The none-

(63) Garrett, B. C.; Truhlar, D. G.; Grev, R. S.; Magnuson, A. W. *J. Phys. Chem.* **1980**, *84*, 1730; **1983**, *87*, 4554E.
(64) Skodje, R. T.; Truhlar, D. G.; Garrett, B. C. *J. Phys. Chem.* **1981**, *85*, 3019.
(65) Truhlar, D. G.; Isaacson, A. D.; Skodje, R. T.; Garrett, B. C. *J. Phys. Chem.* **1982**, *86*, 2252; **1983**, *87*, 4554E.
(66) Isaacson, A. D.; Truhlar, D. G.; Rai, S. N.; Steckler, R.; Hancock, G. C.; Garrett, B. C.; Redmon, M. J. *Comput. Phys. Commun.* **1987**, *47*, 91. Isaacson, A. D.; Truhlar, D. G.; Rai, S. N.; Hancock, G. C.; Lauderdale, J. G.; Truong, T. N.; Joseph, T.; Garrett, B. C.; Steckler, R. University of Minnesota Supercomputer Institute Research Report 88/87, September 1988.

Table XI. Calculated Rate Constants (in cm^3 $molecule^{-1}$ s^{-1}) for Reaction R2 with One or Two Waters

T (K)	conventional TST	CVT	CVT/ MEPSAG	CVT/ SCSAG
		$n = 1$		
250	7.2 (−19)	7.1 (−19)	1.1 (−18)	1.6 (−18)
300	6.4 (−18)	6.3 (−18)	8.3 (−18)	1.1 (−17)
500	8.4 (−16)	8.2 (−16)	9.1 (−16)	1.0 (−15)
1000	9.7 (−14)	9.4 (−14)	9.6 (−14)	9.8 (−14)
		$n = 2$		
250	4.8 (−22)	4.7 (−22)	7.2 (−22)	1.1 (−21)
300	2.1 (−20)	2.0 (−20)	2.7 (−20)	3.7 (−20)
500	7.5 (−17)	7.3 (−17)	8.1 (−17)	9.0 (−17)
1000	1.2 (−13)	1.2 (−13)	1.2 (−13)	1.2 (−13)

Table XII. Calculated CVT/SCSAG Rate Constants k (in cm^3 $molecule^{-1}$ s^{-1}) and Arrhenius Activation Energies E_a (in kcal/mol) for Reaction R1 and for Reaction R2 with One and Two Water Molecules

	R1		R2 ($n = 1$)		R2 ($n = 2$)	
T (K)	k	E_a	k	E_a	k	E_a
200	4.1 (−15)	2.2	1.2 (−19)	4.8	8.4 (−24)	9.3
250	1.4 (−14)	2.6	1.6 (−18)	5.5	1.1 (−21)	10.1
300	3.5 (−14)	3.0	1.1 (−17)	6.0	3.7 (−20)	10.7
400	1.4 (−13)	3.6	1.6 (−16)	6.9	4.1 (−18)	11.8
500	3.6 (−13)	4.1	1.0 (−15)	7.7	9.0 (−17)	12.8
1000	4.2 (−12)	6.0	9.8 (−14)	11.2	1.2 (−13)	16.6

quilibrium solvation rate constants are our best estimates of the true reaction rate constants.

Considering the calculated rate constants given in Table XI, we observe the same trends we saw[41] in the gas-phase reaction R1. Namely, there is little difference between the conventional TST rate constants and the CVT rate constants, and the CVT/SCSAG method predicts a tunneling correction which is roughly twice that predicted by the CVT/MEPSAG method. As discussed in ref 41, the first trend shows that vibrational effects on the location of the dynamical bottleneck are small, while the second trend indicates that there is significant curvature coupling between the reaction coordinate and the generalized normal modes orthogonal to the reaction path.

In order to illustrate the former point, we show the generalized free energy of activation curves at 300 K for reaction R1 and for reaction R2 with $n = 1$ and with $n = 2$ in Figure 3. For each reaction, the CVT transition state occurs at the maximum of the free energy curve, which varies from $s_*^{CVT} = 0.058$ a_0 for the gas-phase reaction to $s_*^{CVT} = 0.050$ a_0 for $n = 1$ and finally to $s_*^{CVT} = 0.046$ a_0 for the $n = 2$ reaction.

Table XI also shows, by dividing column 5 by column 3, that the tunneling effect is essentially independent of the number of waters, $n = 1$ or 2, at all four temperatures.

In Table XII we present rate constants and Arrhenius activation energies calculated by the CVT/SCSAG method. We present results for reaction R2 both with $n = 1$ and $n = 2$, and we also present the results for the gas-phase reaction R1 for comparison. At 200 K the rate for the $n = 1$ reaction is four orders of magnitude slower than the corresponding gas-phase rate, while the $n = 2$ reaction is over eight orders of magnitude slower than its gas-phase analogue. At 300 K, the differences have decreased to three orders of magnitude for the addition of one water and to not quite six orders of magnitude for the addition of two waters. These trends continue until at 1000 K the rates for reaction R2 with $n = 1$ and $n = 2$ are nearly the same, and these rates are only about a factor of 40 slower than that for their gas-phase analogue, reaction R1.

The predicted trends in reactivity are the same as those seen in experimental work on similar microsolvated reactions. Bohme and Raskit[25] and Henchman et al.[27,28] have both measured reaction rates at room temperature for the S_N2 reaction $(H_2O)_n{\cdot}OH^- + CH_3Y$ (and/or its deuterated analogue) where Y is Cl^- or Br^-, and n ranges from 0 to 3, and Bohme and Raskit[26] have measured

Table XIII. Variational TST Rate Constants (in cm^3 $molecule^{-1}$ s^{-1}) for Reaction R2 with One Water ($n = 1$) Calculated under Different Assumptions

		equilibrium solvation	
T (K)	nonequilibrium solvation	solvent-influenced local reaction coordinate	gas-phase local reaction coordinate
200	3.2 (−20)	1.4 (−19)	3.4 (−20)
300	6.3 (−18)	1.9 (−17)	6.8 (−18)
500	8.2 (−16)	1.9 (−15)	9.0 (−16)
1000	9.4 (−14)	1.7 (−13)	1.0 (−13)

rates for the reaction $(D_2O)_n{\cdot}F^- + CH_3Y$, where Y is again Cl^- or Br^-. In all cases, the addition of each additional solvent molecule significantly decreased the reaction rate, although not always monotonically. Bohme and Raskit[25,26] found that less exothermic reactions were slowed more rapidly than more exothermic reactions. In all H_2O analogue reactions they studied, they found over a three-order-of-magnitude decrease in the rate from $n = 0$ to $n = 3$. For the most similar reaction to the one studied here, $(D_2O)_n{\cdot}F^- + CH_3Cl$, the reaction rate was observed to drop two orders of magnitude from the gas phase to $n = 1$, and with the addition of another solvent molecule it became immeasurably slow, indicating a drop of more than another order of magnitude.

For these exothermic reactions both studies[25,27,28] for the OH^- as nucleophile with $n = 1$ showed that the unsolvated ion, Y^-, was formed preferentially over the solvated ion. Bohme et al. found that this outcome is correlated with exothermicity; they found more solvated product ions in less exothermic reactions.[25] For example, in the reaction of $(H_2O){\cdot}OH^-$ with CH_3Br they found only 10% solvent retention,[25] whereas for the reaction of $(D_2O){\cdot}F^-$ with CH_3Cl, solvated ions were the dominant product.[26] Henchman et al.[29] use the significant formation of Br^- as evidence that the $(H_2O){\cdot}OH^- + CH_3Br$ reaction definitely does not proceed by solvent transfer followed by Walden inversion and likely does not proceed in a concerted fashion (followed by dissociation of excited $(H_2O){\cdot}Br^-$); rather, they suggest that it proceeds by Walden inversion followed either by solvent transfer or by solvent dissociation (presumably concurrently with the Br^- dissociation), with the solvent dissociation pathway dominating. They argue that the sequential pathway is preferred over the concurrent pathway, because the concurrent transition state will be entropically less favorable. Because the reaction we have studied is thermoneutral, and no large amount of excess energy is available, the unsolvated ion is less likely to be a significant product, independent of reaction pathway. An efficient solvent transfer has been observed recently by Baer et al.[67] in the approximately thermoneutral reaction $RO^-(HOR) + HCOOR' \rightarrow (R'O^-)(HOR) + HCOOR$.

The question whether the pathway is concurrent or sequential may depend on the number of water molecules, and—in addition—there is not a precise distinction since the two types of mechanism may be combined in intermediate cases. Our potential model exhibits concurrent motions of water transfer and solute inversion at the saddle point; yet at a point on the MEP where the solute is nearly at the geometry of the ion–dipole complex, the water has moved only as much as the leaving chlorine, and it still must rotate to the far side of the leaving chloride, a much larger amplitude motion, in order to reach the potential minimum.

6.2. Test of Equilibrium Solvation Models. As discussed in section 4, we have evaluated the reaction rate for reaction R2 with one water molecule ($n = 1$) under the assumption of equilibrium solvation, and we have used two models for the generalized transition state which differ in the method used to choose the orientation of the hyperplane that divides reactants from products. The variational TST rate constants for both equilibrium solvation calculations as well as those for the nonequilibrium solvation calculations are given in Table XIII. The two equilibrium solvation calculations are distinguished by the nature of the local

(67) Baer, S.; Stoutland, P. O.; Brauman, J. I. *J. Am. Chem. Soc.* **1989**, *111*, 4097.

reaction coordinate used to define the generalized transition state, i.e., the solvent-influenced local reaction coordinate or the gas-phase local reaction coordinate, as described in section 4.2.

The results in Table XIII are quite striking. We see immediatey that the two equilibrium methods of treating solvation give significantly different results. We see only a very small, possibly insignificant, difference between the nonequilibrium-solvation rate constants and the equilibrium-solvation ones calculated with the gas-phase local reaction coordinate. Specifically, the extra recrossing at the equilibrium solvation variational transition state increases the rate constant by less than 10% compared to the full variational calculation over the whole 200–1000 K range. For the solvent-influenced local reaction coordinate though, we see a large increase in the equilibrium solvation rate constants, as compared to the nonequilibrium solvation rate constants. Recrossing of the variational transition state yields an increase in the computed rate constant by a factor of over 4 at 200 K, a factor of more than 3 at 300 K, and factors of 2.3–1.8 at 500–1000 K.

Since we can find a good variational transition state corresponding to equilibrium solvation, we conclude that nonequilibrium solvation effects are small for this reaction and that the gas-phase local reaction coordinate is also reasonable in the presence of hydration. We also conclude that the solvent-influenced local reaction coordinate does not provide a good basis for defining transition states.

The first conclusion, that nonequilibrium effects are small, is a central result of this study. In assessing the significance of this result, it is important to stress that the solvent molecule *is* strongly coupled to the reaction process. For example, the imaginary frequency at the saddle point on the full-dimensionality potential surface for the reaction with one water is 584i cm^{-1}, which is a 25% increase over the imaginary frequency at the gas-phase saddle point, which is 469i cm^{-1}. Also, the coordinates of the nonequilibrium solvation MEP for this reaction show that in the barrier region the extent of motion of the water molecule is of the same magnitude as the motion of the solute atoms. (Hwang et al.[17] also found, in a study involving 60 water molecules, that the solvent motion is of the same magnitude as that of solute atoms.) The picture of the descent from the saddle point that emerges in the present work is that as one CCl bond length shortens, the other one lengthens, the methyl hydrogens move toward the leaving chlorine, and the water molecule (see Figure 1e) remains nearly a constant distance from the leaving chlorine. This indicates that, because of the rapid charge switching at the saddle point, the water molecule is quickly more strongly associated with the leaving chlorine than with the original hydrated chlorine. Thus, we learn that strong solute–solvent coupling does not necessarily mean that nonequilibrium solvation effects are important; rather, the importance of these effects will depend also on dynamic effects such as the relative time scales of the solute reactive motion and the bath motion.

The conclusion that the solvent-influenced local-reaction-coordinate method provides a poor variational transition state for the equilibrium solvation calculations, while the gas-phase gradient method provides a good variational transition state, is also worthy of discussion. On first thought one might expect exactly the opposite result. It might seem in the absence of calculations that the solvent-influenced local reaction coordinate would be more relevant to the reaction in the presence of the solvent than the gas-phase local reaction coordinate would be. However, for simple reactive systems in the gas phase Koeppl[68] has studied the effect of using different local reaction coordinates to define the orientations of generalized transition states at $s = 0$, and he found that, when the generalized-transition-state vibrations are defined by their character in the near vicinity of the reaction path, the best local reaction coordinate to use is the vector associated with the imaginary frequency at the saddle point, which is tangent to the MEP at this point ($s = 0$). He also found that using a more globally defined reaction path to define the local reaction coordinate at $s = 0$ yielded good results in some cases. Gas-phase calculations which consider generalized transition states with $s \neq 0$, but with the MEP defining the local reaction coordinate, have shown that this choice of local reaction coordinate is usually quite good.[31,62] Thus, by analogy to gas-phase reactions, the best generalized transition states are expected to be those which are orthogonal to the reaction path, i.e., for which the reaction path is the local reaction coordinate. For a nonequilibrium solvation calculation the MEP, which is the reaction path, is defined as the local reaction coordinate, making the generalized transition state orthogonal to the MEP. Thus, in that case, the reaction path, the MEP, and the local reaction coordinate coincide. For an equilibrium solvation reaction, we define the ESP as the reaction path. The solvent-influenced gradient, which we choose as the local reaction coordinate in one calculation, does not necessarily point along the ESP; in reality, it tends to point partly in the direction from the ESP to the MEP of the full-dimensionality potential and partly in the direction along the ESP. Which direction forms the greater component of the solvent-influenced gradient, and thus of the solvent-influenced local reaction coordinate, varies along the ESP; in the vicinity of the point on the ESP which corresponds to the gas-phase saddle point, this gradient is dominated by the component which points toward the true MEP.

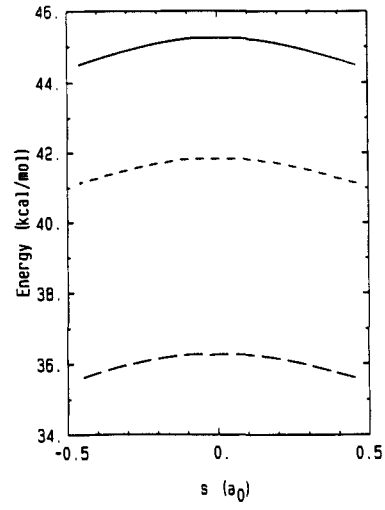

Figure 3. Free energy of activation curves parameterized by the distance along the reaction path s for the gas-phase calculations and for the nonequilibrium solvation variational transition state theory calculations: solid line is $n = 2$, short dashed line is $n = 1$, long dashed line is $n = 0$.

The gas-phase gradient, which defines the gas-phase local reaction coordinate, is not guaranteed to point along the ESP either, but in the reaction considered here it appears to do so. In fact, it seems plausible that the degree to which the gas-phase gradient does point along the ESP will generally be correlated to the validity of the equilibrium solvation assumption for a given reaction. However, more work is required even to know if the method employed here will provide good variational transition states for other reactions (or for R2 with $n > 1$) under the equilibrium solvation assumption.

In Figure 4 we present the free energy of activation curves at 300 K for the nonequilibrium solvation method and for both equilibrium solvation methods. These curves are parameterized by distance along the reaction path, s. For all calculations s is distance along the MEP through the primary system (solute) mass-scaled coordinate system. Figure 4 illustrates the similarity between the nonequilibrium solvation results and the gas-phase local reaction coordinate equilibrium solvation results. The solute-influenced local reaction coordinate method yields quite a different free energy of activation curve. At points in the near vicinity of $s = 0$ this curve is undefined in the harmonic approximation because one of the frequencies of the generalized transition state at these s values is imaginary. This indicates that, at these s values, the ESP corresponds to a ridge in potential energy, rather than a valley, along the coordinate associated with this frequency, a situation which would yield a high density of states and a low value for V_{min}; consequently, the curvature in the

(68) Koeppl, G. W. *J. Am. Chem. Soc.* **1974**, *96*, 6539.

Table XIV. Variational Transition States at 300 K for Reaction R2 with One Water (n = 1) for Different Methods of Calculation[a]

	nonequilibrium solvation[b]			equilibrium solvation: solvent-influenced local reaction coordinate[c]			equilibrium solvation: gas-phase local reaction coordinate[d]		
	x	y	z	x	y	z	x	y	z
				Coordinates					
C	0.000	0.000	0.000	0.000	0.000	0.000	0.000	0.000	0.000
Cl	−0.088	0.000	4.354	0.000	0.000	4.431	0.000	0.000	4.350
H	2.025	0.000	0.013	2.020	0.000	0.079	2.022	0.000	0.000
H	−0.997	−1.759	0.015	−1.010	−1.749	0.079	−1.011	−1.751	0.000
H	−0.997	1.759	0.015	−1.010	1.749	0.079	−1.011	1.751	0.000
Cl′	−0.088	0.000	−4.323	0.000	0.000	−4.263	0.000	0.000	−4.350
H	−4.866	0.000	1.437	−4.788	0.000	1.685	−4.838	0.000	1.425
H	−4.865	0.000	−1.410	−4.892	0.000	−1.162	−4.838	0.000	−1.425
O	−5.996	0.000	0.013	−5.969	0.000	0.301	−5.968	0.000	0.000
				$\hat{g}$					
C	−0.000	0.000	0.822	0.007	0.000	0.790	0.000	0.000	0.822
Cl	0.020	0.000	−0.325	0.075	0.000	−0.225	0.000	0.000	−0.403
H	0.001	0.000	−0.001	−0.027	0.000	−0.007	0.000	0.000	−0.006
H	−0.001	−0.001	−0.001	−0.065	0.064	−0.007	0.000	0.000	−0.006
H	−0.001	0.001	−0.001	−0.065	−0.064	−0.007	0.000	0.000	−0.006
Cl′	−0.019	0.000	−0.466	0.076	0.000	−0.545	0.000	0.000	−0.403
H	0.000	0.000	−0.002	0.000	0.000	0.000	0.000	0.000	0.000
H	−0.000	0.000	−0.002	0.000	0.000	0.000	0.000	0.000	0.000
O	0.000	0.000	−0.010	0.000	0.000	0.000	0.000	0.000	0.000

[a] Although s measures distance in mass-scaled coordinates, we convert the geometries and vector components in this table to unscaled Cartesians to facilitate interpretation. [b] $s_*^{CVT}(a_0)$ = 0.05 a_0. [c] $s_*^{CVT}(a_0)$ = 0.27 a_0. [d] $s_*^{CVT}(a_0)$ = 0.00 a_0.

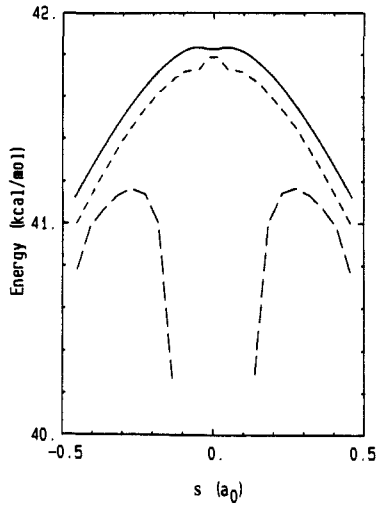

Figure 4. Same as Figure 3, except for the reaction with one water and for (solid line) the nonequilibrium solvation calculation, (short dashed line) the gas-phase local reaction coordinate equilibrium solvation calculation, and (long dashed line) the solvent-influenced local reaction coordinate equilibrium-solvation calculation.

free energy of activation curve, which indicates that the maximum of this curve is not in this undefined region, is correct, and going beyond the harmonic approximation so that we could evaluate the free energy of activation in this region would not change our results. We note that the ESP can correspond to a potential maximum (in some number of dimensions) in the generalized transition state because the generalized transition-state surface is defined over all but one degree of freedom, while the minimization of the solvent coordinates is performed with fixed solute coordinates.

An explicit comparison of the variational transition states (at 300 K) for the three different methods—nonequilibrium solvation, solvent-influenced local reaction coordinate equilibrium solvation, and gas-phase local reaction coordinate equilibrium solvation—is given in Table XIV. Each transition state is completely defined by the set of Cartesian coordinates which give the geometry at s_*^{CVT} on the reaction path and the local reaction coordinate vector $\hat{g}$ at this point; the z axis is the Cl–C–Cl′ axis. For the canonical variational transition state for each method we have listed s_*^{CVT}, the Cartesian coordinates at s_*^{CVT} (in a_0), and $\hat{g}$ at s_*^{CVT}. The variational transition state for the solvent-influenced local reaction coordinate calculation occurs much further along the reaction path, at s_*^{CVT} = 0.27 a_0, than do the variational transition states for the other two methods, which have s_*^{CVT} near the saddle point (s = 0), and this is reflected in the coordinate sets. At the solvent-influenced local reaction coordinate variational transition state, the water molecule (last three rows of the coordinates in Table XIV) is shifted 0.3 a_0 away from the carbon toward the leaving chlorine (Cl), and the chlorines are shifted a comparable amount from their symmetric saddle point configuration; the other two transition-state structures show a large amount of symmetry around z = 0. Another important aspect of the transition-state structures is that the nonequilibrium solvation transition-state structure shows a nonzero x component for both chlorines, whereas the equilibrium solvation transition-state structures do not. This is because the fully optimized one-water saddle point has a bent Cl–C–Cl structure (see section 3.3), whereas the gas-phase saddle point has a collinear Cl–C–Cl structure. For reaction R2, however, the rates appear to be governed by the orientation of the transition state, which is defined by the local reaction coordinate $\hat{g}$.

One important point about the local reaction coordinates is that for the equilibrium solvation transition states the local reaction coordinate has zero magnitude in the solvent coordinates by definition. These coordinates have small magnitudes in the nonequilibrium solvation local reaction coordinate as well, despite the fact that for noninfinitesimal motions the water motion is of the same order of magnitude as the chlorine motions (compare the z coordinates of the equilibrium solvation path at s = 0.27 a_0 with those at s = 0.00 a_0; the z-coordinate motion is quite similar on the nonequilibrium solvation path). The major components, the solute z-coordinate components, are of similar size for all three local reaction coordinates. Comparing the nonequilibrium solvation local reaction coordinate with the equilibrium solvation gas-phase local reaction coordinate, we see little difference, with the variances localized to the x coordinates which are small in the first case but zero in the latter. The equilibrium solvation solvent-influenced local reaction coordinate has significantly larger x components than the other two local reaction coordinates, with difffering signs. These components correspond to the ClCCl′ bend and in-plane methyl hydrogen distortions. These are exactly the motions by which the gas phase and the fully optimized one-water saddle point differ from each other, supporting the idea that the equilibrium solvation solvent-influenced local reaction coordinate includes a significant component in the direction from the ESP

Table XV. Harmonic Frequencies in cm^{-1} for the Generalized Transition State at $s = 0.18$ a_0 for Three Different Calculations

	equilibrium solvation	
nonequilibrium solvation	solvent-influenced local reaction coordinate	gas-phase local reaction coordinate
47	42	43
92	89	92
114	118	118
205	208	208
212	(165)[a]	218
238	230	231
327	325	325
363	367	367
423	419	419
947	947	947
949	950	950
1026	1025	1026
1384	1384	1384
1388	(1133)[a]	1389
1702	1699	1700
3105	3037	3105
3307	3307	3307
3309	3308	3309
3751	3751	3751
3854	3855	3855

[a] Parentheses indicate frequencies which are changed significantly from the nonequilibrium solvation values. For these modes, correspondence was determined by an eigenvector analysis.

to the nonequilibrium solvation MEP.

Table XV lists the frequencies of the modes in the generalized transition state defined by $s = 0.18$ a_0 for each of the three methods. As in the rate constant results, there are only small changes between the frequencies of the nonequilibrium-solvation generalized transition state and those of the equilibrium-solvation gas-phase-local-reaction-coordinate generalized transition state at $s = 0.18$ a_0, indicating that indeed there is a similarity between the sequence of generalized transition states for the two methods, at least in the barrier region. The significant differences in the frequency spectra of the solvent-influenced local reaction coordinate method and the nonequilibrium solvation method are confined to two modes. The first of these is the ClCCl bend in the plane of the water molecule. The frequency for this mode in the solvent-influenced local reaction coordinate calculation is 165 cm^{-1}, which is 22% lower than the 212-cm^{-1} frequency of the nonequilibrium calculation. The second is, in the nonequilibrium-solvation calculation, a mode which involves a scissor motion of the two methyl hydrogens which are closest to the water molecule and has a frequency of 1388 cm^{-1}. In the solvent-influenced local reaction coordinate equilibrium solvation calculation, this mode contains a significant asymmetric stretch component which is not present in the nonequilibrium solvation eigenvector, and the frequency is 1133 cm^{-1}, 18% lower than the nonequilibrium solvation value. We also see a mixing of the asymmetric stretch with another methyl hydrogen mode, which involves both the HCH bend of the previous mode as well as a stretch of the other CH bond length, in the solvent-influenced local reaction coordinate results, but the frequency lowering of 68 cm^{-1} is only a 2% change from the nonequilibrium solvation value of 3105 cm^{-1}. The configuration of the solute on the MEP and the solute on the ESP differ by a ClCCl bend and an expansion of the HCH angle which is bisected by the water monomer; the reaction path motion near the saddle point is largely the solute asymmetric stretch. These results clearly indicate that, indeed, the solvent-influenced generalized transition state is defined by a local reaction coordinate which is some combination of a vector which points from the ESP to the MEP and a vector which points along the ESP path toward reactants.

7. Discussion

From the preceding analysis (section 6.2), it can be seen that the calculated rate constant is lowered by rotating the generalized transition-state hyperplane so that it includes higher frequency modes, leaving lower frequency motion along the local reaction coordinate. High-frequency motion corresponds to fast motion of light particles (and short distances in mass-scaled coordinates), while low-frequency motion corresponds to slow motion of heavy particles (and long distances in mass-scaled coordinates). Thus, the rate constant decreases when the generalized transition state is rotated such that faster motions lie in the transition state, and consequently relatively slower motions occur along the local reaction coordinate. The variationally optimal transition state, which minimizes the calculated rate constant, will thus be oriented such that relatively slow motions are included in the local reaction coordinate. Therefore if slow motions are excluded from the local reaction coordinate, the generalized transition-state theory rate constant will be too high. In effect, excluding slow motions from the local reaction coordinate will cause recrossings of a transition state defined by this local reaction coordinate. Thus, if the slow time scale motions are motions of bath molecules which are not being used in defining the local reaction coordinate because of an equilibrium solvation approximation, they would be expected to induce recrossings of the transition state. However, these recrossings can be reduced or eliminated by including some or all of these slow motions in the local reaction coordinate, i.e., by rotating the generalized transition state into the solvent degrees of freedom. Within this formulation, then, nonequilibrium-solvation effects are those recrossings which can be eliminated *only* by including solvent motions in the local reaction coordinate. Recrossing effects which can be eliminated by changing the orientation of the local reaction coordinate *within* the solute coordinate space do not constitute a breakdown of the equilibrium solvation assumption; rather they indicate a poor choice of dividing surface within this framework. This shows how the formalism presented here provides a way to quantify the qualitative notion that slow-solvent motions and fast reaction-coordinate motion cause the equilibrium solvation approximation to break down. In addition it shows that the extent to which solvation is judged to be equilibrated or not depends on the choice of the local reaction coordinate.

The above argument also leads to new insights into the deficiencies of the simple time scale arguments; in particular it does not include the coupling strengths between various motions or the relation between the local reaction coordinate and the global reactive motion in which one is interested. Thus, orienting the transition state orthogonal to the lowest frequency mode will not provide a good bottleneck to reaction if this mode is truly a spectator to the reaction of interest. The strength of the coupling between slow time scale motions and the mode which most directly couples reactants to products will determine the degree to which these slow motions should be included in the local reaction coordinate. Much work is necessary, however, before we will understand these relationships in detail.

Several previous studies of the aqueous-phase analogue of reaction R1 have been reported. In such cases the number of bath coordinates make it impractical to find the ESP in the manner used here, and so both the reaction coordinate and the local reaction coordinate were defined only in terms of solute coordinates, not including bath coordinates. In one approach, because separable mode approximations based on a single potential minimum may be very poor for systems containing many solvent molecules, eq 7 was used [rather than eq 8] to evaluate the rate constant, and statistical techniques were used to consider the effects of solvation on the free energy of activation. In particular, Chandrasekhar et al.[8] used Monte Carlo techniques to evaluate the free energy along a reaction path, and Chiles and Rossky[21] and Huston et al.[21] have used an extended RISM method to evaluate the free energy along a slightly different reaction path. Bergsma et al.[12] have gone to yet a third formulation of TST, that of trajectories crossing a dividing surface, i.e., a generalized transition state. They used molecular dynamics to choose initial conditions for the trajectories, so that the ensemble of trajectories considered represents an equilibrium distribution at the generalized transition state for a given temperature. In order to understand the relevance of our results to such studies, we would have to answer the following questions for each study: First, in what way

has the equilibrium solvation assumption been used, and second, what degree of freedom has been removed from the generalized transition state, i.e., how is the local reaction coordinate defined. Some of the previous work, however, defines the local reaction coordinate only implicitly. In addition, it is necessary to recast discussions in terms of solvent friction[1-3,12,13,69,70] into the language of free energy of activation and the solvent's contribution thereto, as discussed for example by Gertner et al.[13]

It is especially interesting to compare our conclusions to those of Gertner et al.[12,13,19] and Huston et al.[21] because they have evaluated a recrossing factor and attributed the recrossing to nonequilibrium solvation effects. As evidence that the observed recrossing is due to solvent friction, i.e., nonequilibrium solvation effects, Gertner et al.[12,13,19] have shown that they can account for the recrossing of the dividing surface, i.e., the generalized transition state, seen in the trajectory calculations with a generalized Langevin equation approach.[2,16,34,38-40,71] In their most recent work, they evaluate transmission coefficients κ defined as

$$\kappa = \frac{k}{k^{TST}} \tag{10}$$

where k here represents the "true" nonequilibrium solvation rate constant, evaluated by a classical mechanical simulation, and k^{TST} is a "standard" transition-state theory rate constant evaluated under the equilibrium solvation approximation.[19] They also evaluated κ by the generalized Langevin approach of Grote and Hynes[71] (GH) and compared the two sets of results. In the GH approach the transmission coefficient is given by[19]

$$\kappa_{GH} = \frac{\lambda_r}{\omega_{b,Eq}} \tag{11}$$

where λ_r is the frequency for barrier crossing including dynamical solvent effects, and $\omega_{b,Eq}$ is the equilibrium barrier frequency, i.e., the frequency for barrier crossing under the assumption of equilibrium solvation. This frequency, $\omega_{b,Eq}$, is defined by making the assumptions that the maximum of the free energy of activation curve occurs at the saddle point and that this curve is parabolic. In the notation of section 4 this definition implies

$$\max_s[\Delta G^{GT,0}_{298}] = \Delta G^{GT,0}_{298}(s = 0) \tag{12}$$

and

$$\Delta G^{GT,0}_{298} = -\frac{1}{2}\mu\omega^2_{b,Eq}s^2 \tag{13}$$

where the local reaction coordinate is assumed (chosen) to be coincident with the reaction path. The first condition, eq 12, is often a poor assumption[31,35] although it is usually better for reactions with high barriers, as studied here. From eq 11 it is clear that κ_{GH} depends upon the frequency of equilibrium barrier crossing, $\omega_{b,Eq}$, predicted under the assumptions given by eqs 12 and 13. The validity of these assumptions as well as the value obtained for k^{TST} in eq 10 is dependent on the choice of local reaction coordinate. Gertner et al.[12,13,19] used the relationships for $\omega_{b,Eq}$ derived by van der Zwan and Hynes[39] to evaluate it from molecular dynamics simulations. Thus, the choice of local reaction coordinate is made implicitly by imposing a constraint on the molecular dynamics simulation. Specifically, the local reaction coordinate is determined by the procedure for choosing an equilibrium distribution of trajectory initial conditions. This distribution implicitly defines the generalized transition state. In particular the local reaction coordinate is defined by requiring the scalar distance $r_{as} \equiv {}^1/_2 r_c$ to remain equal to zero during the initial equilibration of the trajectories. This defines a surface in which the solvent coordinates and other solute coordinates are equilibrated, but this surface is not a hyperplane orthogonal to the imaginary frequency normal mode; in the event that the imaginary frequency *is* the asymmetric stretch at the point defined by $r_{as} = 0$ with all other coordinates optimized, this hyperplane will be *tangent* to the curvilinear surface defined by the constraint $r_{as} = 0$. The constraint $r_{as} = 0$ defines a curvilinear surface because r_{as} is a difference of interparticle separations. It is quite possible that this curvilinear dividing surface provides an adequate bottleneck; however, such surfaces have never been tested, even for gas-phase calculations where the equilibrium solvation assumption is unnecessary. Finally, by using the constraint $r_{as} = 0$, it is implicitly assumed that this point ($s = 0$) defines the maximum of the free energy of activation curve for an optimum or nearly optimum shape and orientation of the dividing surface, and, consequently, that the generalized transition state defined by this constraint provides a good bottleneck to reaction (in the equilibrium solvation assumption); we have shown that this is not necessarily a good assumption (see Figure 4). It would be very interesting to test whether the recrossing that Gertner et al.[12,13,19] find in their trajectory calculations and successfully reproduce with the generalized Langevin theory could be reduced or eliminated by varying the generalized transition state used in the trajectory calculations.

Huston et al.[21] evaluated the transmission coefficient in the nonadiabatic (NA) limit of the generalized Langevin theory; the transmission coefficient in this limit, which is called κ_{NA}, may be evaluated by a simple approximation of van der Zwan and Hynes[38-40] which does not require a molecular dynamics simulation to evaluate any of the necessary quantities. In their calculations[21] $\omega_{b,Eq}$ is evaluated from a free energy of activation curve using eq 13 at $s = 0$. In the application to the chloride plus methyl chloride system, Huston et al. found a transmission coefficient of 0.6, which they interpreted as a measure of solvent-induced recrossing. We can check the applicability of the nonadiabatic limit formula by evaluating κ_{NA} from the present calculations by using[13,39]

$$\kappa_{NA} = \frac{\omega_{b,NA}}{\omega_{b,Eq}} \tag{14}$$

where $\omega_{b,NA}$ is evaluated as in eq 13 but using the nonequilibrium (i.e., full) calculation of $\Delta G^{GT,0}_{298}$ rather than the equilibrium solvation curve. We evaluated effective frequencies from the upper two curves in Figure 4; since these curves are not globally quadratic we fit them by using points at the maximum and the distance where $\Delta G^{GT,0}_{300} \cong \max \Delta G^{GT,0}_{300} - RT$, which should be the important region for thermally activated reactions. This yields $\kappa_{NA} = 0.92$, in very good agreement with the full calculations, which yield a nonequilibrium solvation effect of 0.93 by using the ratio of 300K rate constants in Table XIII. This increases the credibility of this simple approximation for the nonequilibrium solvation effect, so we may compare our calculations to those of Huston et al. with more confidence. We conclude therefore that the nonequilibrium solvation effect in bulk water is somewhat larger, 40% vs. 10%, for bulk water than for the monohydrated reaction. We note, though, that in the work of Huston et al. the free energy associated with the solute degrees of freedom which are orthogonal to the solute coordinate used to define the "free energy of activation curve" is neglected. It would be interesting to learn, e.g., by repeating their calculations including all degrees of freedom of the primary system, what effect these extra constraints have on the evaluated curvature of the free energy curve, and consequently, upon the calculated value of κ for bulk water. The potential function presented in this paper would be a suitable starting point for such a calculation.

Van der Zwan and Hynes[39,40] and Pollak[72] have shown that the effects accounted for[71] by generalized Langevin theory for systems with harmonic baths and bilinear solute–solvent coupling may also be accounted for by rotating the generalized transition-state theory reaction coordinate from being strictly within the solute coordinates to having components in the full solute–solvent space. This type of rotation is discussed in the first paragraph of this section. In a system with higher order couplings the analytic theory breaks down. Our calculations include nonlinear solute–solvent couplings

(69) Kramers, H. A. *Physica* **1940**, *7*, 284.
(70) Takeyama, N. *Experientia* **1971**, *17*, 425.
(71) Grote, R. F.; Hynes, J. T. *J. Chem. Phys.* **1980**, *73*, 2715.
(72) Pollak, E. *J. Chem. Phys.* **1986**, *85*, 865.

and optimize not only the orientation of the generalized transition-state dividing surface but also its location with respect to translation along the reaction path.

It would also be interesting to compare our approach to that of Hwang et al.[17] Hwang et al.[17] calculated a free energy of activation profile as a function of a reaction coordinate defined as the difference in energy of two diabatic states representing the charge-transfer processes. The result is independent of the gas-phase reaction path. In the language used here this is a nonequilibrium-solvation variational transition-state theory calculation. It would be interesting to see how much the variational transition-state rate constant is changed in their model by introducing the equilibrium solvation assumption for a gas-phase reaction path. It would also be interesting to apply their approach to cluster reactions such as considered here to elucidate the connection between their reaction coordinate and ours and between their free energy function and our generalized free energy of activation.

8. Conclusions

The semiempirical potential energy function of the preceding paper, augmented by a water intramolecular potential and a water–solute interaction potential, has been used to study the chloride plus methyl chloride bimolecular nucleophilic substitution reaction in the presence of one and two water molecules, including all degrees of freedom. A noteworthy feature of the potential function used here is that we include reaction coordinate dependent force constants and partial charges for all atoms of the solute. For both the monohydrated and dihydrated reactions, we found that as the reaction proceeds the water molecules migrate from the approaching chloride to the leaving chloride. At the charge–dipole complex, we found that the reactant microhydrated chloride ion forms a weak bond to the methyl chloride with almost no change to the solvent–ion configuration and that rotation of the solvent–ion complex around the methyl chloride C–Cl axis has virtually no energy barrier, less than 0.0005 kcal/mol for one water molecule and ~0.003 kcal/mol for two water molecules.

With the addition of just two water molecules, we see a definite trend toward the solution-phase reaction profile. For example, the barrier height, relative to reactants as zero of energy, increases from a value of 3.1 kcal/mol in the gas phase, to 5.4 kcal/mol for the monohydrated reaction, and to 10.7 kcal/mol for the dihydrated reaction, as compared to the accepted value of the solution phase barrier of 26.6 kcal/mol. These trends are mirrored in the reaction rates (calculated by the CVT/SCSAG method) which, at 300 K, decrease from 3.5×10^{-14} cm^3 molecule^{-1} s^{-1} in the gas phase, to 1.1×10^{-17} cm^3 molecule^{-1} s^{-1} for the monohydrated reaction, to 3.7×10^{-20} cm^3 molecule^{-1} s^{-1} for the dihydrated reaction. These trends are consistent with those seen experimentally for stepwise hydration of similar systems.

We have also studied the monohydrated reaction under the equilibrium solvation assumption and have shown by comparison to the nonequilibrium solvation rate that a strong solute–solvent coupling does not *necessarily* mean that nonequilibrium solvation effects will be important. For the monohydrated reaction the imaginary frequency at the saddle point is 584i cm^{-1}, 25% higher than the gas phase value of 469i cm^{-1}, and the associated eigenvector shows a component indicating that the water molecule moves with the leaving chlorine. Yet, an equilibrium solvation calculation employing the gas-phase local reaction coordinate leads to less than a 10% increase in the rate constant, for all temperatures considered, as compared to the nonequilibrium solvation rate constant, indicating no significant amount of solvent-induced recrossing. This is consistent with the work of van der Zwan and Hynes[39] who concluded that a fast solvent strongly coupled to the solute can lead to negligible nonequilibrium effects.

We presented two methods for choosing the orientation, defined by the local reaction coordinate, of the generalized transition state in an equilibrium solvation calculation: the solvent-influenced local reaction coordinate method and the gas-phase local reaction coordinate method. (Both are consistent with the criterion that in an equilibrium-solvation calculation the local reaction coordinate—and thus the *orientation* of the generalized transition state—should be defined in the solute coordinate space only.) We found that the amount of recrossing of the canonical variational generalized transition state, determined by comparison to the nonequilibrium solvation rate constants, differed dramatically for the two methods. The solvent-influenced local reaction coordinate method showed a significant increase in the rate constant due to recrossing of the generalized transition state, ranging from a factor of 4.5 at 200 K to a factor of 3.0 at 300 K and a factor of 1.8 at 1000 K, whereas the gas-phase local reaction coordinate method, which is the variationally better choice, showed less than a 10% increase in the rate constant for all temperatures. Thus we conclude that caution must be exercised in drawing conclusions about nonequilibrium solvation effects when a particular way of modelling equilibrium solvation does not agree with a more complete dynamical calculation. In particular recrossing caused by a poor choice of the generalized transition state must be distinguished from recrossing caused by a breakdown of the equilibrium solvation assumption. The generalized transition state theory formulation presented here provides a useful theoretical framework for more precise discussions of these dynamical effects, and the variational criterion for the choice of the best generalized transition state provides a practical way to find the best equilibrium solvation model.

Stated another way, even if there are no nonequilibrium solvation effects, an equilibrium solvation calculation will not necessarily agree with a full—i.e., nonequilibrium solvation—calculation because there is more than one way to translate the equilibrium solvation assumption into transition-state language, and they are not all equally accurate. We used variational transition-state theory to choose the better of two possible ways to define local reaction coordinates corresponding to equilibrium solvation. We found that equilibrium solvation is a good approximation for the case considered since one way of incorporating the equilibrium solvation assumption in generalized transition-state theory is valid to within 8%, although another way is only valid to within about a factor of 3. Thus one must distinguish the failure of the equilibrium solvation approximation from the failure of a less than optimum way of implementing it.

Acknowledgment. We are grateful to Doreen Leopold and Steven Kass for providing useful references. This work was supported in part by the U.S. Department of Energy, Office of Basic Energy Sciences.

Registry No. Cl^-, 16887-00-6; CH_3Cl, 74-87-3.

Supplementary Material Available: Listings of parameters for the short-range solute–water potential, V^{SB}, and of Cartesian coordinates for the $n = 1$ and $n = 2$ stationary points discussed in section 3 (2 pages). Ordering information is given on any current masthead page.